8 Transducer Sound Radiation

In this Chapter, we will examine models that can describe the radiated sound field generated by an ultrasonic transducer and some of the important parameters that govern the behavior of that field. We will demonstrate most of these results for immersion transducers but many of the concepts introduced also are valid for contact transducers as well. We will also discuss some of the major differences between immersion and contact transducers.

8.1 An Immersion Transducer as a Baffled Source

Figure 8.1 (a) shows a circular planar (non-focused) immersion transducer radiating into a fluid medium, where we have placed the face of the transducer in the *x*-*y* plane so that it is pointing in the positive *z*-direction. When this transducer is driven by the pulser the underlying piezoelectric crystal will move. That motion, in turn, will produce a transient velocity field on the face of the transducer which we will assume is a normal motion (in the *z*-direction). This velocity field we will write as $v_z(x,y,t)$. Since the pulser drives the transducer with a very short voltage pulse, the motion of the face of the transducer that is generated by this excitation will also be a short time duration pulse. However, we will not model this mechanical motion directly, but instead will deal with its Fourier transform, $v_z(x,y,\omega)$. Such a frequency domain response can alternately be viewed as the result of assuming that the velocity field on the face of the transducer has a harmonic motion given by $v_z = v_z(x,y,\omega)\exp(-i\omega t)$ which generates a radiated sound pressure field in the fluid given by $p(x,y,z,\omega)\exp(-i\omega t)$. Since all the variables for harmonic motion problems have the same common time factor, $\exp(-i\omega t)$, it is customary to drop this time factor and assume it implicitly, a convention we will often follow here.

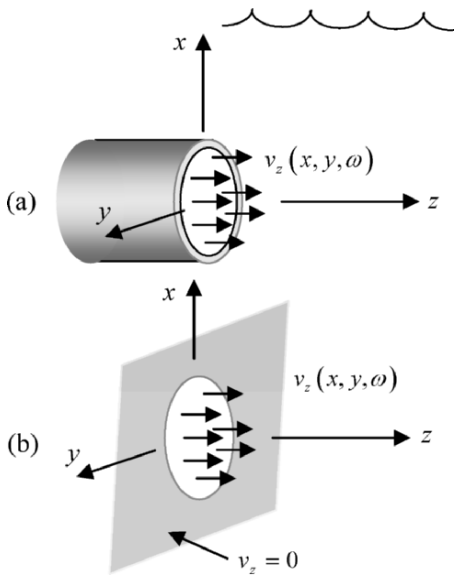

Fig. 8.1. (a) A planar immersion transducer radiating waves into a fluid produced by a harmonic velocity field $v_z(x,y,\omega)$ on its face, and **(b)** a transducer model consisting of the same velocity field in (a) surrounded by a motionless baffle on the z = 0 plane.

Most transducer models do not directly deal with the geometry of Fig. 8.1 (a) but instead consider the alternate geometry of Fig. 8.1 (b) where it is assumed that there is an infinite plane at $z = 0$ over which the velocity is specified [Fundamentals]. On the surface, S, of the transducer, which lies in this plane, the velocity is given as $v_z = v_z(x,y,\omega)$. For the remainder of the plane one takes $v_z = 0$. These conditions would correspond to having the transducer face embedded in an infinite, motionless, plane baffle. This modified geometry should still represent well our original problem, however, since the transducer will generate a sound field that is significant only in the region ahead of the transducer anyway and the actual fields in the fluid on the plane z = 0 outside of the surface S will be very small, if not identically zero. Mathematically it is more convenient to use the baffled geometry of Fig. 8.1 (b) rather than the original geometry since we then need only to find how a specified velocity field on $z = 0$ generates fields in the fluid half-space $z > 0$.

Determining what the velocity field distribution is on the face of a commercial transducer is not a trivial task. Although in principle it is

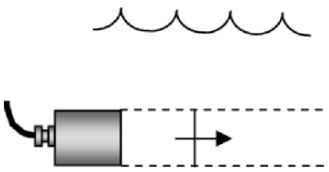

Fig. 8.2. A transducer radiating a perfectly collimated beam at high frequencies.

possible to determine this field experimentally, the measurements are time-consuming and require expensive equipment. Fortunately, for many commercial transducers we can avoid this difficulty by assuming a velocity distribution. The most common assumption is to treat the transducer as a *piston transducer* where the velocity is taken to be spatially uniform over the entire transducer face, i.e. $v_z(x,y,\omega) = v_0(\omega)$. This simple piston model has proven to work well as a basis for characterizing many commercial transducers so it is the model we will adopt here. One should be aware that the validity of this assumption, however, depends on the construction details of the transducer and may be violated in some cases.

If the frequency, ω, was infinitely large a transducer would emit a beam of sound that is confined only to the cylinder of fluid $z \geq 0$, $r \leq a$ ahead of the transducer as shown in Fig. 8.2. Such a beam is said to be perfectly *collimated*. In reality the frequency is not infinite so that the beam will spread beyond this cylinder, but at the MHz frequencies found in NDE testing a transducer beam will still remain fairly well collimated. This fact is demonstrated in Fig. 8.3 where the magnitude of the pressure

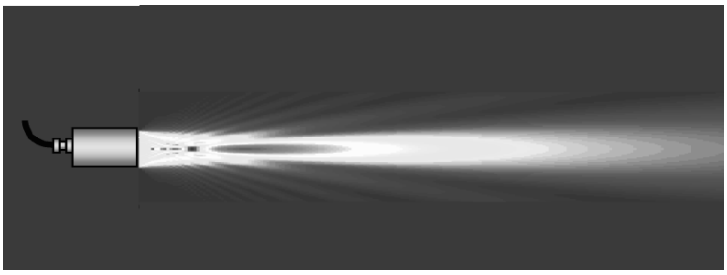

Fig. 8.3. A 5 MHz, ½ inch diameter circular piston transducer radiating sound into water.

field in the *x*-*z* plane is shown for a one half inch radius planar piston transducer radiating at 5 MHz into water. There are strong pressure variations in the pressure field, particularly in the region near the transducer. These variations show that one cannot consider the transducer beam to be a simple uniform and well collimated beam as seen, for example, in a flashlight beam. Modeling these pressure variations, therefore, is a non-trivial task.

8.2 An Angular Plane Wave Spectrum Model

Although a transducer does not generate only a plane wave, one way to model a transducer (as a baffled source) is to treat it as the superposition of an infinite number of plane waves, all traveling in the positive *z*-direction but with different *x*- and *y*- component directions. This is basic idea behind an *angular plane wave spectrum model*, where the pressure wave field at a point, $\mathbf{x} = (x, y, z)$, is represented in the form of a 2-D integral given by [Fundamentals], [8.1]

$$p(\mathbf{x},\omega) = \left(\frac{1}{2\pi}\right)^2 \int_{-\infty}^{+\infty}\int_{-\infty}^{+\infty} P(k_x, k_y)\exp\left[i\left(k_x x + k_y y + k_z z\right)\right] dk_x dk_y. \tag{8.1}$$

Since the time-domain pressure, $p(\mathbf{x},t)$, must satisfy the 3-D wave equation

$$\frac{\partial^2 p}{\partial x^2} + \frac{\partial^2 p}{\partial y^2} + \frac{\partial^2 p}{\partial z^2} - \frac{1}{c^2}\frac{\partial^2 p}{\partial t^2} = 0 \tag{8.2}$$

for $p(\mathbf{x},t) = p(\mathbf{x},\omega)\exp(-i\omega t)$ we must have $p(\mathbf{x},\omega)$ satisfy

$$\frac{\partial^2 p}{\partial x^2} + \frac{\partial^2 p}{\partial y^2} + \frac{\partial^2 p}{\partial z^2} + k^2 p = 0, \tag{8.3}$$

which is called the *Helmholtz equation*. Clearly, $p(\mathbf{x},\omega)$ will satisfy Eq. (8.3) if all of the exponential terms in Eq. (8.1) also satisfy that equation. Placing $\exp\left[i\left(k_x x + k_y y + k_z z\right)\right]$ into Eq. (8.3), we find as a requirement that $k_z = \pm\sqrt{k^2 - k_x^2 - k_y^2}$. In order to have waves traveling in the positive *z*-direction (as they must, physically, for our problem), only

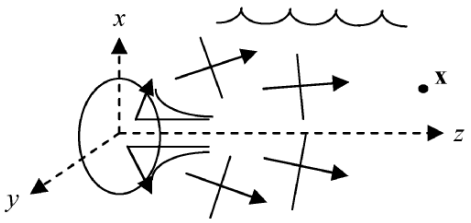

Fig. 8.4. Model of a transducer as a superposition of plane and inhomogeneous waves radiating into the region $z \geq 0$.

the positive value is acceptable and so we choose $k_z = \sqrt{k^2 - k_x^2 - k_y^2}$. Terms such as $p = \exp\left(ik_x x + ik_y y + i\sqrt{k^2 - k_x^2 - k_y^2}\, z\right)$ are just plane harmonic waves as long as $k^2 > k_x^2 + k_y^2$ is satisfied. In Eq. (8.1), however, all values of k_x, k_y are superimposed so that there will be values of those variables in the integrations where $k_x^2 + k_y^2 > k^2$ and k_z will be imaginary. For those cases if we take $k_z = i\sqrt{k_x^2 + k_y^2 - k^2}$ we will no longer have plane waves propagating into the half-space $z > 0$ but instead will have waves that propagate in the x- and y-directions from the transducer but that are exponentially decaying in the z-direction of the form $p = \exp\left(ik_x x + ik_y y - \sqrt{k_x^2 + k_y^2 - k^2}\, z\right)$ [note: $k_z = -i\sqrt{k_x^2 + k_y^2 - k^2}$ cannot be used since then we would obtain waves that grow exponentially in the z-direction away from the transducer, which is not physical]. Such waves are called *inhomogeneous waves.* Thus, strictly speaking, Eq. (8.1) represents the pressure wave fields as a superposition of both plane wave and inhomogeneous wave fields (see Fig. 8.4) where we must have

$$k_z = \begin{cases} \sqrt{k^2 - k_x^2 - k_y^2}, & k^2 \geq k_x^2 + k_y^2 \\ i\sqrt{k_x^2 + k_y^2 - k^2}, & k^2 < k_x^2 + k_y^2 \end{cases}. \tag{8.4}$$

Appendix D gives a discussion of inhomogeneous waves found when solving plane wave transmission/reflection problems.

In order for Eq. (8.1) to represent the solution to our baffled transducer model, we must determine the unknown $P\left(k_x,k_y\right)$ so that the velocity boundary conditions are satisfied on the plane $z = 0$. From the equation of motion for the fluid (see Appendix D) we have

$$v_z\left(x,y,z=0,\omega\right)=\frac{1}{i\omega\rho}\frac{\partial p}{\partial z}\left(x,y,z=0,\omega\right), \tag{8.5}$$

where ρ is the density of the fluid. Placing Eq. (8.1) into this relationship we find

$$\begin{aligned} v_z\left(x,y,z=0,\omega\right)=\left(\frac{1}{2\pi}\right)^2\int_{-\infty}^{+\infty}\int_{-\infty}^{+\infty}\frac{ik_zP\left(k_x,k_y\right)}{i\omega\rho} \\ \cdot\exp\left[i\left(k_xx+k_yy\right)\right]dk_xdk_y \end{aligned} \tag{8.6}$$

To see what Eq. (8.6) means, let $V\left(k_x,k_y\right)=ik_zP\left(k_x,k_y\right)/i\omega\rho$. Then Eq. (8.6) becomes simply

$$\begin{aligned} v_z\left(x,y,z=0,\omega\right)=\left(\frac{1}{2\pi}\right)^2\int_{-\infty}^{+\infty}\int_{-\infty}^{+\infty}V\left(k_x,k_y\right) \\ \cdot\exp\left[i\left(k_xx+k_yy\right)\right]dk_xdk_y. \end{aligned} \tag{8.7}$$

Equation (8.7) is in the form of two inverse Fourier transforms where the t and ω parameters in the time and frequency domains (see Appendix A) are replaced by wave numbers and spatial parameters, i.e. $\omega\rightarrow k_x,-t\rightarrow x$ for one transform and $\omega\rightarrow k_y,-t\rightarrow y$ for the other transform. Thus, Eq. (8.7) is called an inverse 2-D *spatial* Fourier transform. By the properties of the Fourier transform it then follows that we must have

$$V\left(k_x,k_y\right)=\int_{-\infty}^{+\infty}\int_{-\infty}^{+\infty}v_z\left(x,y,z=0,\omega\right)\exp\left[-i\left(k_xx+k_yy\right)\right]dxdy, \tag{8.8}$$

which shows that $V\left(k_x,k_y\right)$ is just the 2-D spatial Fourier transform of the velocity field on the plane $z = 0$. For a circular piston transducer of radius a, for example, where

$$v_z\left(x,y,z=0,\omega\right)=\begin{cases}v_0\left(\omega\right) & x^2+y^2\le a^2\\ 0 & x^2+y^2>a^2\end{cases} \tag{8.9}$$

the 2-D spatial Fourier transform in Eq. (8.8) can be obtained explicitly as

$$V\left(k_x,k_y\right)=2\pi a^2 v_0\left(\omega\right)\frac{J_1\left(\sqrt{k_x^2+k_y^2}\,a\right)}{\sqrt{k_x^2+k_y^2}\,a}, \tag{8.10}$$

where J_1 is a Bessel function of order one. Similarly, for a rectangular piston transducer of length l_x in the x-direction and length l_y in the y-direction we find

$$V\left(k_x,k_y\right)=l_x l_y v_0\left(\omega\right)\frac{\sin\left(\frac{k_x l_x}{2}\right)\sin\left(\frac{k_y l_y}{2}\right)}{\left(\frac{k_x l_x}{2}\right)\left(\frac{k_y l_y}{2}\right)}. \tag{8.11}$$

Thus, for any given velocity distribution on $z = 0$, the pressure wave field from the transducer can be found explicitly as

$$\begin{aligned} p\left(\mathbf{x},\omega\right)=\left(\frac{1}{2\pi}\right)^2\int_{-\infty}^{+\infty}\int_{-\infty}^{+\infty}\frac{i\omega\rho\,V\left(k_x,k_y\right)}{ik_z} \\ \cdot\exp\left[i\left(k_x x+k_y y+k_z z\right)\right]dk_x dk_y \end{aligned} \tag{8.12}$$

once the 2-D spatial Fourier transform of the velocity field at $z = 0$ is known. Equation (8.12) is an exact result that can be used directly for numerical modeling of transducer wave fields. However, it is a model that is numerically very challenging to implement since one still needs to perform two infinite integrations of rapidly varying functions. In practice, it has been found that the inhomogeneous waves contribute little to the pressure wave field except in a region very close to the transducer, which is usually not of great interest. Thus, most numerical evaluations of Eq. (8.12) simply ignore all the inhomogeneous waves and compute instead the finite integrals over all the plane wave terms

$$\begin{aligned} p\left(\mathbf{x},\omega\right)=\left(\frac{1}{2\pi}\right)^2\iint_{k_x^2+k_y^2\le k^2}\frac{i\omega\rho V\left(k_x,k_y\right)}{ik_z} \\ \cdot\exp\left[i\left(k_x x+k_y y+k_z z\right)\right]dk_x dk_y. \end{aligned} \tag{8.13}$$

Equation (8.13) is now a more tractable transducer model, but it still requires a significant amount of computation (i.e. many plane wave

components need to be superimposed) in order to adequately simulate the transducer beam. Also, Eq. (8.13) does not explicitly show us much about the physics of the sound generation process. Thus, we will consider another transducer model that remedies some of these deficiencies.

8.3 A Rayleigh-Sommerfeld Integral Transducer Model

In discussing linear systems in Appendix C, we saw that the convolution theorem played a crucial role. In that case, we showed that a 1-D time domain convolution of two functions was equivalent to taking the inverse Fourier transform of a product of their Fourier transforms. Since here Eq. (8.12) is in the form of a 2-D inverse spatial Fourier transform of a product of 2-D transforms, we could expect that a 2-D form of the convolution theorem might play an equally important role here. This indeed turns out to be the case. First, we state the following 2-D (spatial) convolution theorem [8.2]:

If

$$f(x,y)=\left(\frac{1}{2\pi}\right)^2\int_{-\infty}^{+\infty}\int_{-\infty}^{+\infty}H(k_x,k_y)G(k_x,k_y)\exp\left[i\left(k_x x+k_y y\right)\right]dk_x dk_y$$

then

$$f(x,y)=\int_{-\infty}^{+\infty}\int_{-\infty}^{+\infty}h(x',y')g(x-x',y-y')dx'dy'$$

where $H(k_x,k_y)$ is the 2-D spatial Fourier transform of $h(x,y)$ and $G(k_x,k_y)$ is the 2-D spatial Fourier transform of $g(x,y)$. We can use this theorem directly for Eq. (8.12) if we make the following definitions

$$\begin{aligned} H(k_x,k_y) &= -i\omega\rho\, V(k_x,k_y) \\ G(k_x,k_y) &\equiv G(k_x,k_y,z)=\frac{\exp(ik_z z)}{-ik_z}. \end{aligned} \tag{8.14}$$

Then it follows that

$$h(x,y) = -i\omega\rho v_z(x,y,z=0,\omega)$$
$$g(x,y) \equiv g(x,y,z) = \frac{\exp\left[ik\sqrt{x^2+y^2+z^2}\right]}{2\pi\sqrt{x^2+y^2+z^2}}. \tag{8.15}$$

The expression for h in Eq. (8.15) follows directly from the fact that $V(k_x,k_y)$ is the 2-D spatial Fourier transform of $v_z(x,y,z=0,\omega)$. The expression for g in Eq. (8.15) comes from Weyl's representation of a spherical wave in terms of an angular plane wave spectrum integral [Fundamentals]. In particular, Weyl showed that

$$\begin{aligned}
&\frac{\exp\left[ik\sqrt{x^2+y^2+z^2}\right]}{2\pi\sqrt{x^2+y^2+z^2}} \\
&= \left(\frac{1}{2\pi}\right)^2 \int_{-\infty}^{+\infty}\int_{-\infty}^{+\infty} \frac{1}{-ik_z} \exp\left[i\left(k_x x + k_y y + k_z z\right)\right] dk_x dk_y \\
&= \left(\frac{1}{2\pi}\right)^2 \int_{-\infty}^{+\infty}\int_{-\infty}^{+\infty} \frac{\exp(ik_z)}{-ik_z} \exp\left[i\left(k_x x + k_y y\right)\right] dk_x dk_y.
\end{aligned} \tag{8.16}$$

From Eqs. (8.12), (8.14) and (8.15) and the 2-D convolution theorem then it follows that we have an alternate representation for the pressure wave field of a transducer given by

$$\begin{aligned}
p(\mathbf{x},\omega) = \frac{-i\omega\rho}{2\pi} \int_{-\infty}^{+\infty}\int_{-\infty}^{+\infty} v_z(x',y',z=0,\omega) \\
\cdot \frac{\exp\left[ik\sqrt{(x-x')^2+(y-y')^2+z^2}\right]}{\sqrt{(x-x')^2+(y-y')^2+z^2}} dx'dy',
\end{aligned} \tag{8.17}$$

which is called the *Rayleigh-Sommerfeld integral*. Just as Eq. (8.12) gave us a transducer model in terms of a superposition of plane (and inhomogeneous) waves traveling in different directions, the Rayleigh-Sommerfeld integral represents the transducer radiation as a superposition of spherical waves radiating from point sources distributed on the plane $z = 0$. Since any transducer only generates a non-zero velocity over some finite area, S, (see Fig. 8.5), we can rewrite Eq. (8.17) more compactly as

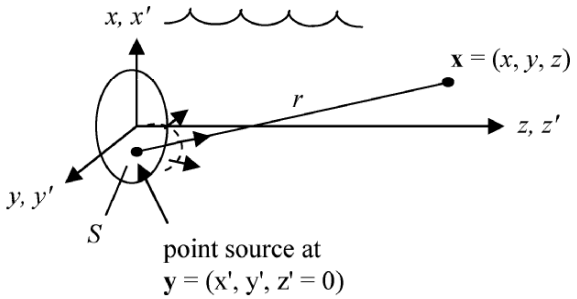

Fig. 8.5. A transducer modeled as a superposition of radiating point sources.

$$p(\mathbf{x},\omega) = \frac{-i\omega\rho}{2\pi}\iint_S v_z(x',y',z=0,\omega)\frac{\exp(ikr)}{r}dS \tag{8.18}$$

where $r = \sqrt{(x-x')^2 + (y-y')^2 + z^2}$ (see Fig. 8.5) is the distance from an arbitrary point $\mathbf{y} = (x',y',0)$ on the transducer surface, S, to a point, $\mathbf{x} = (x,y,z)$, in the fluid and dS is an element of area on the transducer surface. For the particular case of a piston transducer the Rayleigh-Sommerfeld integral reduces to an even simpler form given by

$$p(\mathbf{x},\omega) = \frac{-i\omega\rho\, v_0(\omega)}{2\pi}\iint_S \frac{\exp(ikr)}{r}dS. \tag{8.19}$$

The Rayleigh-Sommerfeld integral for a piston source, Eq. (8.19), is used in many texts to discuss transducer radiation in a fluid [Fundamentals]. In general, it still requires a significant amount of numerical effort to evaluate since although one now only has to integrate over the finite face of the transducer, the complex exponential term in the integrand of Eq. (8.19) has a rapidly varying phase for the frequencies and transducer sizes used in NDE tests that makes the 2-D numerical integrations lengthy. However, as we will see, the Rayleigh-Sommerfeld integral does allow us to examine more directly the physics of the transducer radiation problem than Eq. (8.12) permits and we can even extract exact results in some important special cases.

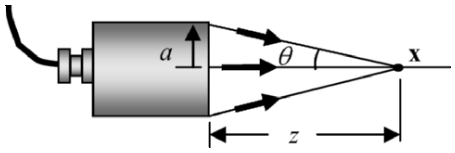

Fig. 8.6. Geometry for a circular planar piston transducer radiating direct and edge waves to a point **x** on the axis of the transducer.

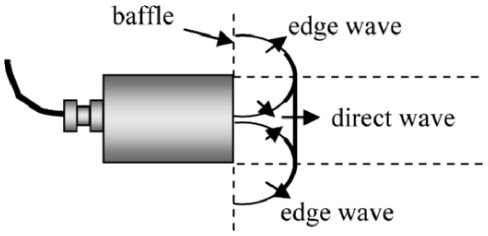

Fig. 8.7. The direct and edge waves generated by an impulsively excited circular piston transducer.

8.4 On-Axis Behavior of a Planar Circular Piston Transducer

Consider first the special case where we wish to obtain the pressure wave field on the central axis of a circular piston transducer of radius a as shown in Fig. 8.6. In this case because of symmetry we can take the area element as $dS = 2\pi\rho_0 d\rho_0$, where ρ_0 is the radial distance on the plane $z = 0$ from the center of the transducer to an arbitrary point on the transducer surface. Since $r^2 = \rho_0^2 + z^2$ it follows that $dS = 2\pi r dr$. Placing this result into Eq. (8.19) then allows us to integrate the remaining complex exponential term to obtain an exact expression for the on-axis pressure given by [Fundamentals]

$$p(z,\omega) = \rho c v_0(\omega)\left[\exp(ikz) - \exp\left(ik\sqrt{z^2 + a^2}\right)\right]. \tag{8.20}$$

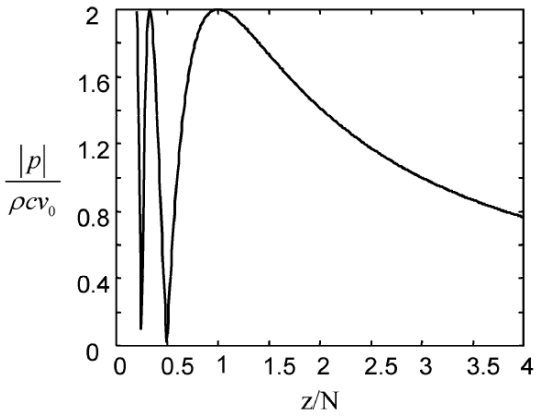

Fig. 8.8. On-axis normalized pressure versus normalized distance *z/N* for a 5 MHz, 1/2 inch diameter planar transducer radiating into water, where *N* is the near field distance.

The first term is a wave that has traveled a distance z directly from the face of the transducer to the point on the transducer axis while the second term is a wave that has traveled a distance $\sqrt{z^2 + a^2}$ so that it appears to have come from the edge (rim) of the transducer, as shown in Fig. 8.6. Indeed, if one examines the pulses which travel from an impulsively excited transducer, as shown in Fig. 8.7 , one sees a plane wave front (the "direct" wave) that travels normal to the face of the transducer and a doughnut-like wave front that comes from the transducer rim (the "edge" wave). Except very near the transducer and for very short pulses, however, we will likely not see these two waves separately. Indeed, at large distances from the transducer where $z >> a$, an expansion of the edge wave term gives $\sqrt{z^2 + a^2} \approx z\left[1 + a^2 / 2z^2\right]$. If we also assume $ka^2 / 2z << 1$ it follows to first order that

$$p(z,\omega) = \frac{-i\omega\rho a^2 v_0(\omega)}{2} \frac{\exp(ikz)}{z}, \tag{8.21}$$

which now looks like a single, spherically spreading wave. This result is reasonable since at sufficiently large distances from the transducer the transducer should act like a point source. Distances that satisfy this criterion are said to be in the *transducer far field* or in the spherically spreading region of the transducer.

If one plots the magnitude of the on-axis pressure versus z that one obtains from Eq. (8.20), then one sees two distinct types of behavior for the on-axis response (Fig. 8.8). Near the transducer one sees a series of nulls and maxima. In this near field region, one can show from Eq. (8.20) that the maxima are located approximately at the distances $z = N/(2m+1) \quad m = 0,1,2,...$ while the nulls are at approximately $z = N/2n \quad n = 1,2,3,...$ where $N = a^2/\lambda$ (the ratio of the radius squared of the transducer to the wave length, λ) is called the *near field distance* and distances $z < N$ are said to be in the *transducer near field* [Fundamentals]. As the distance z increases, the last on-axis null occurs at $z = N/2$ and the last on-axis maximum occurs at $z = N$. Beyond $z = N$ the pressure field simply decays monotonically. At a distances greater than approximately three near field distances from the transducer the exact on-axis response begins to agree very well with the far field expression of Eq. (8.21) so that $z = 3N$ is generally taken as the start of the *transducer far field* region.

8.5 The Paraxial Approximation

Having the exact on-axis behavior of the transducer also enables us to discuss an important concept called the *paraxial approximation*. If we examine the direct and edge waves we see (Fig 8.6) that they are separated by the angle θ. At a distance z approximately equal to a transducer diameter ($2a$), this angle begins to become small enough so that we can assume $\sqrt{z^2 + a^2} \approx z\left[1 + a^2/2z^2\right]$. However, unlike the far field case, we will not also assume $ka^2/2z << 1$ (which is equivalent to $z >> \pi N$, i.e. under this condition we must be many near field distances away from the transducer), so that we are not necessarily in the transducer far field. This means that in the present case we are only assuming that the angle θ is small enough so that all the waves in the transducer beam can be considered to be traveling in approximately the same direction (which in this case is along the z-axis). This is the essence of the paraxial approximation. For this approximation we have

$$p(z,\omega) = \rho c v_0 \exp(ikz)\left[1 - \exp\left(\frac{ika^2}{2z}\right)\right]. \tag{8.22}$$

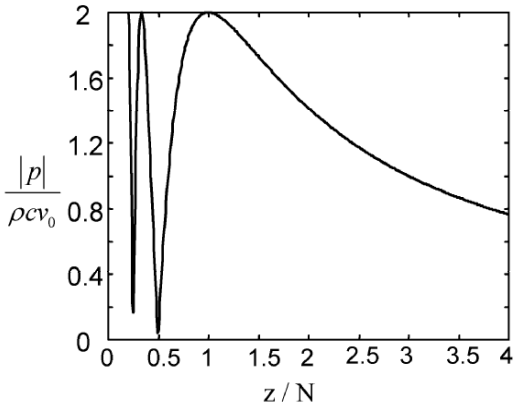

Fig. 8.9. On-axis normalized pressure versus normalized distance *z/N* for a 5 MHz, 1/2 inch diameter planar transducer radiating into water (paraxial approximation).

Equation (8.22) still contains the direct and edge waves of the original exact response but it is in the form of a quasi-plane wave since it can be written as

$$p(z,\omega) = C(z,a,\omega)\left[\rho c v_0 \exp(ikz)\right]. \tag{8.23}$$

The term in the brackets in Eq. (8.23) is just a plane wave traveling in the *z*-direction. The coefficient $C(z,a,\omega)$ that multiplies this plane wave is called a *diffraction coefficient*. It accounts for all the deviations in amplitude and phase of the on-axis response in the actual transducer beam from that of a plane wave. In this case we simply have

$$C(z,a,\omega) = 1 - \exp\left(ika^2/2z\right). \tag{8.24}$$

Figure 8.9 plots the on-axis response in the paraxial approximation (Eq. (8.22)) for the same case shown in Fig. 8.8. It can be seen from those figures that the paraxial approximation captures well both the near and far field on-axis behavior of the transducer. Only within approximately a transducer diameter, a region not shown in these figures, does the paraxial approximation begin to lose accuracy. This means that for most NDE testing situations where we are not concerned with the wave fields immediately adjacent to the transducer, the paraxial approximation should work well. The importance of the paraxial approximation is that it can also work well in much more general testing situations where we are considering

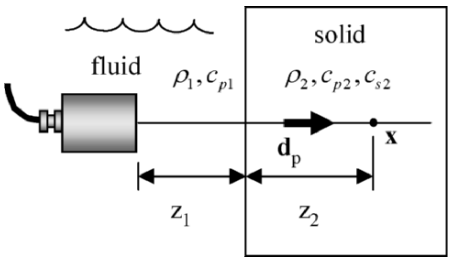

Fig. 8.10. An immersion transducer radiating at normal incidence through a planar fluid-solid interface.

off-axis transducer responses and where the transducer beam itself has been transmitted or reflected from various parts of a component's geometry. These types of complicated interactions occur frequently in NDE tests, so that if the paraxial approximation is valid, we may still treat the sound beam approximately as a quasi-plane wave and all the complicated interactions of the transducer sound beam with the component geometry can be treated approximately as interactions of a plane wave with that geometry. Plane wave interactions are much easier to deal with than interactions involving more general wave types so that the paraxial approximation gives us a powerful tool for accurately simulating many complex problems. The key, of course, is in being able to efficiently determine the diffraction coefficient (either analytically or numerically) for a given testing problem. Fortunately, this is possible, as we will see, in many cases. We will outline here one example where the paraxial approximation can be used in a more general testing setup to determine the transducer wave field. Consider a planar circular piston transducer of radius *a* radiating through a planar fluid-solid interface at normal incidence (see Fig. 8.10). In this case the compressional waves (P-waves) in the fluid generate primarily P-waves in the isotropic elastic solid and the on-axis velocity in the solid is given by [Fundamentals]

$$\mathbf{v}\left(z_2,\omega\right)=v_0T_{12}^{P;P}\mathbf{d}_p\exp\left(ik_{p1}z_1+ik_{p2}z_2\right)\left[1-\exp\left(\frac{ik_{p1}a^2}{2\tilde{z}}\right)\right], \tag{8.25}$$

where $k_{pj}=\omega/c_{pj}\ \left(j=1,2\right)$ are wave numbers for P-waves in the fluid and solid, respectively, $\mathbf{d}_p$ is a unit vector (polarization vector) along the

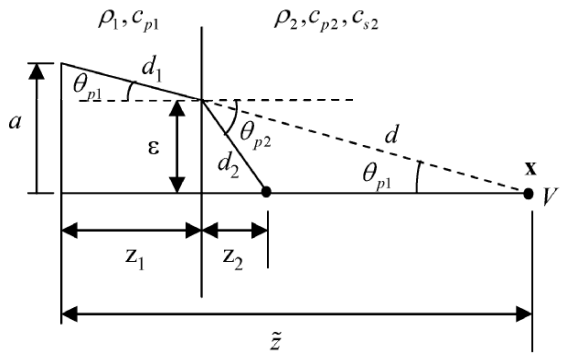

Fig. 8.11. Propagation of an edge wave through a fluid-solid interface to an on-axis point **x** in the solid and the corresponding "virtual" point *V* that the edge wave would travel to in the solid if it's angle was not changed upon refraction through the interface.

propagation direction, $T_{12}^{P;P}$ is a plane wave transmission coefficient for P-waves in the solid due to P-waves in the fluid (the ratio of the velocity at the interface on the solid side to the velocity on the fluid side) and $\tilde{z} = z_1 + c_{p2} z_2 / c_{p1}$. The combined leading terms multiplying the bracketed expression in Eq. (8.25) represent a plane wave that has traveled from the transducer to a depth, z_2, in the solid while the bracketed term itself is the diffraction coefficient for this problem. Interestingly, this diffraction coefficient is in exactly the same form as for the on-axis response for a single fluid medium so that all of the near and far field on-axis behavior we discussed previously for the single fluid case remain valid for this problem if we replace the *z*-distance in the fluid by the equivalent distance $z_1 + c_{p2} z_2 / c_{p1}$. This result can be explained by the behavior of the edge wave at the interface as shown in Fig. 8.11. From that figure we see that $\varepsilon = d_2 \sin\theta_{p2} = d \sin\theta_{p1}$ where d_2 is the path length of the edge wave in the solid and *d* is the distance from the interface to a "virtual" point, *V*, on the axis of the transducer in the solid, which is where the edge wave would arrive on the axis if it had not had its direction changed upon refraction. Solving for *d*, we find $d = d_2 \sin\theta_{p2} / \sin\theta_{p1}$. However, from Snell's law for refracted waves we have $\sin\theta_{p2} / \sin\theta_{p1} = c_{p2} / c_{p1}$ so $d = \left(c_{p2} / c_{p1}\right) d_2$. If we now define the corresponding distance to the virtual point along the *z*-axis as $\tilde{z}$, in the paraxial approximation this virtual point distance is given

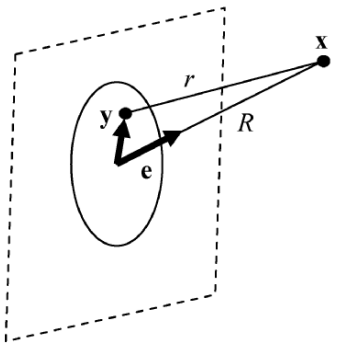

Fig. 8.12. Geometry parameters for defining the far field behavior of a transducer.

by $\tilde{z} \cong d_1 + d = d_1 + \left(c_{p2}/c_{p1}\right) d_2 \cong z_1 + \left(c_{p2}/c_{p1}\right) z_2$. We see that for the interface problem, in the paraxial approximation the refracted waves appear to go through a z-distance, $\tilde{z}$, to the virtual point on the axis in exactly the same manner as for a single medium problem where the interface is absent. In the diffraction correction for a single medium, therefore, one can simply replace the z-distance by the equivalent distance, $\tilde{z}$, to obtain the diffraction correction for this case.

8.6 Far field On-Axis and Off-Axis Behavior

In section 8.4 we obtained an explicit expression (Eq. (8.21)) for the on-axis far field wave field of a circular planar piston transducer. Here, we will show that it is possible to obtain an expression for the entire far field transducer behavior for both on- and off-axis points for planar transducers. This expression is often referred to as the *Fraunhoffer approximation* for the transducer wave field. First, we express the radius r in Eq. (8.18) in terms of the distance R and unit vector $\mathbf{e}$ pointing from the center of the transducer to point $\mathbf{x}$ as (see Fig. 8.12)

$$\begin{aligned} r &= \sqrt{(\mathbf{x}-\mathbf{y})\cdot(\mathbf{x}-\mathbf{y})} \\ &= \sqrt{(R\mathbf{e}-\mathbf{y})\cdot(R\mathbf{e}-\mathbf{y})}. \end{aligned} \tag{8.26}$$

In the far field $|\mathbf{y}| << R$ so we can expand the square root in Eq. (8.26) to obtain:

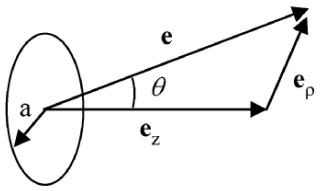

Fig. 8.13. The unit vector, **e**, and its cylindrical components, where $\mathbf{e}_z$ is along the z-axis and $\mathbf{e}_\rho$ is in a radial direction in a plane parallel to the circular transducer of radius *a*.

$$\begin{aligned} r &\cong R\sqrt{1-2\mathbf{e}\cdot\mathbf{y}/R} \\ &\cong R-\mathbf{e}\cdot\mathbf{y}. \end{aligned} \tag{8.27}$$

Both terms in Eq. (8.27) are used to approximate *r* in the phase part of the spherical wave term in Eq. (8.18) while only the leading term is used to approximate the 1/*r* amplitude term. The reason for this difference in the number of terms retained is that the phase is much more sensitive to approximation than the amplitude since in the phase not only must a term that is neglected be smaller than those terms retained but the neglected term must also be much less than 2π. These approximations reduce Eq. (8.18) to the form

$$p(\mathbf{x},\omega)=\frac{-i\omega\rho}{2\pi}\frac{\exp(ikR)}{R}\iint_S v_z(x',y',0,\omega)\exp(-ik\mathbf{e}\cdot\mathbf{y})\,dS, \tag{8.28}$$

which can be rewritten as

$$\begin{aligned} p(\mathbf{x},\omega)=\frac{-i\omega\rho}{2\pi}\frac{\exp(ikR)}{R}\iint_S \{v_z(x',y',0,\omega) \\ \cdot\exp\left[-i\left(k_x x+k_y y\right)\right]dx'dy'\}, \end{aligned} \tag{8.29}$$

where $k_x=ke_x, k_y=ke_y$. From Eq. (8.8) we recognize the integral in Eq. (8.29) as just the 2-D spatial Fourier transform of the velocity field, $V(k_x,k_y)$, so that we have, finally

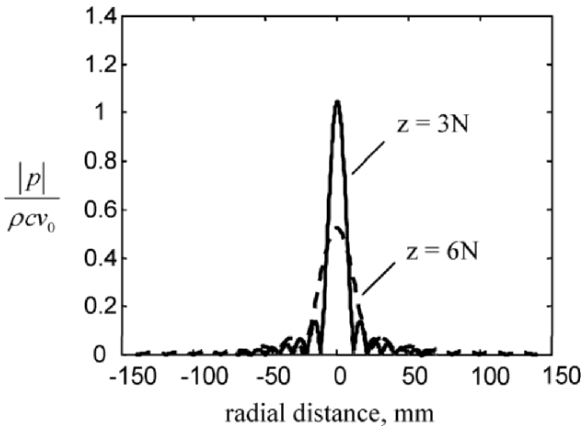

Fig. 8.14. The far field variation of the normalized pressure versus radial distance, ρ_0, for a circular transducer at three and six near field distances, showing the spreading of the angular lobes of the response and the decay in amplitude with increasing distance from the transducer.

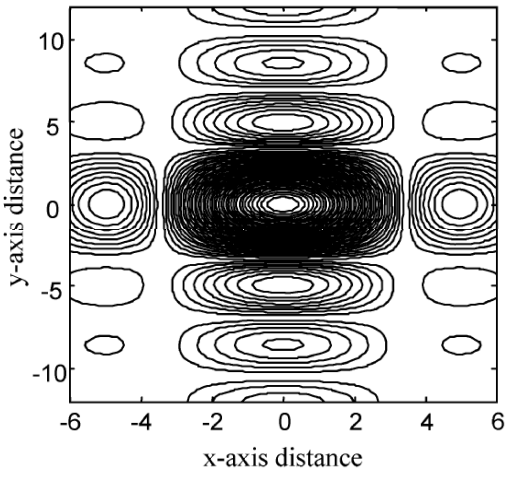

Fig. 8.15. The contours of the far field pressure distribution in a plane parallel to the face of a 3mm x 6 mm rectangular transducer radiating into water at 5 MHz and at a distance of 70 mm.

$$p(\mathbf{x},\omega)=\frac{-i\omega\rho V\left(k_x,k_y\right)}{2\pi}\frac{\exp(ikR)}{R}. \tag{8.30}$$

For a circular piston transducer, we have, using Eq. (8.10) and $e_\rho=\sqrt{e_x^2+e_y^2}=\sin\theta$ (see Fig. 8.13)

$$p(\mathbf{x},\omega)=-i\omega\rho a^2 v_0(\omega)\frac{J_1(ka\sin\theta)}{ka\sin\theta}\frac{\exp(ikR)}{R}, \tag{8.31}$$

which represents a spherical pressure wave in the far field whose amplitude is angular dependent. Figure 8.14 plots the magnitude of the normalized pressure, $|p|/\rho c v_0$, at different fixed distances, z, from the transducer face as a function of the radial distance, ρ_0, from the transducer's central axis, where $\sin\theta=\rho_0/z$. For both $z=3N$ and $z=6N$ one sees the lobe structure generated by the $J_1(u)/u$ angular directivity term of the response in the far field. At $z=6N$, however, the lobes are broader than at $z=3N$ due to beam spreading and the amplitude is also smaller because of the 1/R spherical wave decay term.

For a rectangular transducer with length l_x in the x-direction and length l_y in the y-direction, Eqs. (8.11) and (8.30) give the far field behavior as

$$p(\mathbf{x},\omega)=\frac{-i\omega\rho l_x l_y v_0(\omega)}{2\pi}\frac{\sin(k_x l_x/2)\sin(k_y l_y/2)}{(k_x l_x/2)(k_y l_y/2)}\frac{\exp(ikR)}{R}. \tag{8.32}$$

Figure 8.15 gives a 2-D cross sectional plot of the magnitude of the normalized pressure, $2\pi|p|/\rho c v_0$, as a function of the distances x and y for a given distance z, where $k_x=kx/R=kx/\sqrt{x^2+y^2+z^2}$ and $k_y=ky/R=ky/\sqrt{x^2+y^2+z^2}$. This figure shows the complex 2-D lobe structure present for a rectangular transducer.

8.7 A Spherically Focused Piston Transducer

Many commercial focused transducers produce a focused acoustic sound beam by incorporating an acoustic lens into the transducer design. Modeling

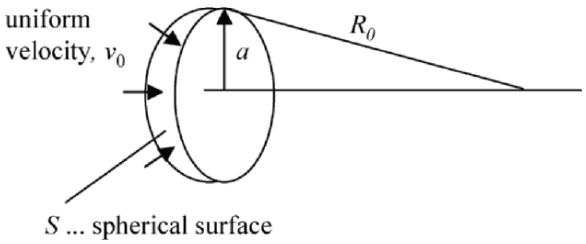

Fig. 8.16. The O'Neil model for a spherically focused piston transducer.

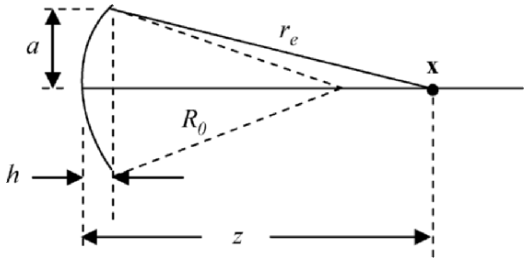

Fig. 8.17. Geometry parameters that appear in the on-axis response of a spherically focused transducer.

in detail such a configuration is very difficult but one can induce the same focusing effect by considering the transducer to be a piston transducer where a constant (radial) velocity is placed on a spherical surface instead of a plane one. In this case one still uses the Rayleigh-Sommerfeld integral (Eq. (8.19)) but now the integration is over a finite radius, a, of a spherical surface S whose radius of curvature is R_0, as shown in Fig. 8.16. This focused transducer model is due to O'Neil [8.3], [Fundamentals]. While the replacement of the integration over a plane surface in the Rayleigh-Sommerfeld integral by integration over a spherical surface is an ad-hoc approach that is not valid in a strict mathematical sense the O'Neil model has been shown to be accurate as long as the focusing is not too severe. Such severe focusing can be found in practice, for example, in acoustic microscopes. Most commercial focused NDE transducers, however, are not tightly focused so that the O'Neil model should work well in practice for most NDE applications. For a point **x** in the fluid on the axis of the spherically focused transducer one

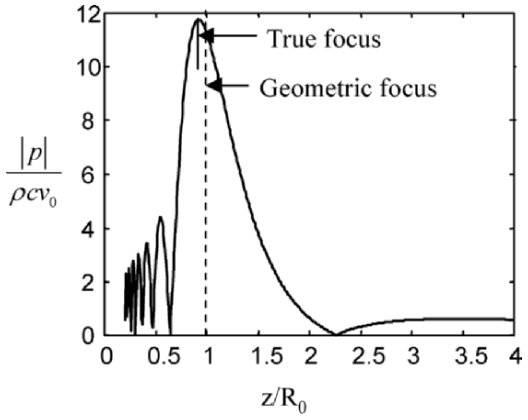

Fig. 8.18. The on-axis normalized pressure for a 6.35 mm radius spherically focused piston transducer radiating into water at 10 MHz with a geometric focal length of 76.2 mm.

can show that the element of area $dS = (2\pi / q_0) r dr$ where $q_0 = 1 - z / R_0$ [Fundamentals]. Thus, the O'Neil model, like the Rayleigh-Sommerfeld model, can be integrated exactly for this case. We find

$$p(z,\omega) = \frac{\rho c v_0}{q_0}\left[\exp(ikz) - \exp(ikr_e)\right], \tag{8.33}$$

where $r_e = \sqrt{(z-h)^2 + a^2}$ and $h = R_0 - \sqrt{R_0^2 - a^2}$. These distances are shown in Fig. 8.17.

Figure 8.18 shows a plot of the normalized pressure, $|p| / \rho c v_0$, versus normalized distance, z / R_0, for a 6.35 mm radius transducer with geometrical focal length of 76.2 mm radiating into water at 10 MHz. It can be seen from that figure that for distances where $z < R_0$ the response has a series of nulls and maxima which eventually produce a single large peak near $z = R_0$ (the geometrical focal length). There is another null at approximately $z = 2.25\, R_0$ and a very small response thereafter. It can be shown that the nulls are located approximately at distances z_n given by [Fundamentals]

$$z_n = R_0\left(\frac{h}{h \pm n\lambda}\right), \tag{8.34}$$

where λ is the wave length and the plus sign is for nulls satisfying $z < R_0$ while the minus sign is for nulls where $z > R_0$. For nulls beyond the geometrical focus, however, there is an additional restriction $h \geq n\lambda$ that must be satisfied for those nulls so that in some cases such nulls may not exist at all. Unfortunately, one cannot write down a simple relationship for the location of the on-axis maxima as done for the planar transducer case. The most one can do is state that they are determined by the roots of a transcendental equation which is [Fundamentals]

$$\cos\left(k\delta/2\right) = \frac{2\left(\delta + z\right)\sin\left(k\delta/2\right)}{kR_0\left(\delta + h\right)q_0}, \tag{8.35}$$

where $\delta = r_e - z = \sqrt{\left(z-h\right)^2 + a^2} - z$.

Note that due to wave diffraction effects the maximum response (true focus) at finite frequencies occurs at a distance somewhat less than the geometric focal length (geometric focus), as shown for this case. It is only at infinitely large frequencies that the maximum on-axis response occurs at $z = R_0$.

With some algebra we can express the distance r_e also in the form $r_e = \sqrt{z^2 + \left(a^2 + h^2\right)q_0} - z$ [Fundamentals]. In the paraxial approximation we must have $h << a$ (not too severe focusing) and $z >> a$ (not too near the transducer). In this approximation we find

$$\begin{aligned} r_e &\cong \sqrt{z^2 + a^2 q_0} - z \\ &\cong z\left(1 + \frac{a^2 q_0}{2z^2} + \ldots\right) - z \\ &= \frac{a^2 q_0}{2z} \end{aligned} \tag{8.36}$$

so that the on-axis response in Eq. (8.33) becomes

$$p\left(z,\omega\right) = \rho c v_0 \exp\left(ikz\right)\left\{\frac{1}{q_0}\left[1 - \exp\left(ika^2 q_0/2z\right)\right]\right\}, \tag{8.37}$$

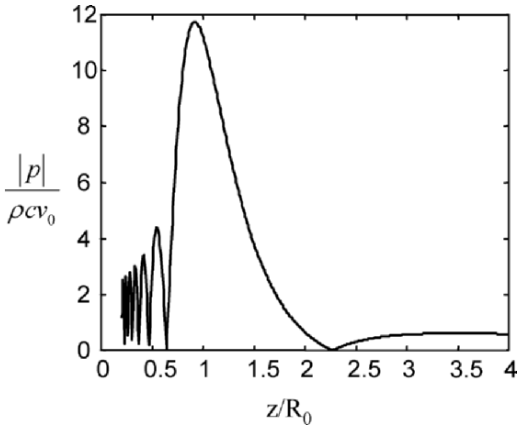

Fig. 8.19. The on-axis response calculated with the paraxial approximation for the same spherically focused transducer shown in Fig. 8.18.

which shows that the on-axis diffraction coefficient for a spherically focused piston transducer is given by

$$C(z,a,R_0,\omega)=\frac{1}{q_0}\left[1-\exp\left(ika^2q_0/2z\right)\right]. \tag{8.38}$$

For a planar transducer $q_0 \to 1$ and Eq. (8.38) reduces to Eq. (8.22). As in the planar case the paraxial approximation works very well in describing the ultrasonic beam from a spherically focused transducer as long as the focusing is not too severe and one is not too close to the transducer. Figure 8.19 shows the on-axis pressure plot predicted in the paraxial approximation for the same case shown in Fig. 8.18. It can be seen that the two responses are nearly identical.

The paraxial approximation also can be used as a means for illustrating a relatively simple way to incorporate focusing into a transducer beam model. Consider a planar circular piston transducer. Since the velocity is uniform over the face of the transducer, the phase of this velocity field is constant (zero) on this aperture. In contrast, if the transducer had generated a spherically converging wave which focuses at z $= R_0$ on the axis of the transducer the phase of the velocity field on the aperture would not be a constant (see Fig. 8.20). On the plane z = 0 we would instead have a phase term given, in the paraxial approximation, by

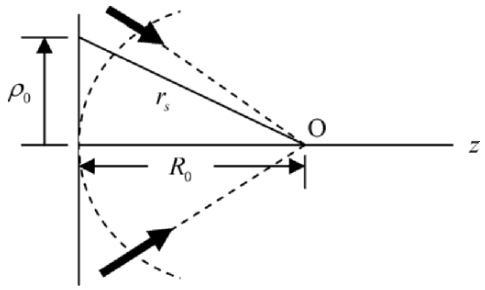

Fig. 8.20. Geometry for defining the phase variations on the plane z = 0 of a spherically converging wave that focuses at z = R_0 .

$$\begin{aligned}&\exp\left(-ik\left[r_s - R_0\right]\right) = \exp\left[-ik\left[\sqrt{\rho_0^2 + R_0^2} - R_0\right]\right] \\ &\cong \exp\left(-ik\rho_0^2 / 2R_0\right).\end{aligned} \tag{8.39}$$

[Note: we have included the ikR_0 term in Eq. (8.39) so that the phase of the wave is zero at the origin $\left(\rho_0 = z = 0\right)$, i.e. the wave starts out from that point at time t = 0. The $-ikr_s$ term has a negative sign because r_s decreases as the time t increases, i.e the wave is a spherical wave converging to point O on the axis]. Now, suppose we take the Rayleigh- Sommerfeld integral model of a planar piston transducer and simply include the phase term given in Eq. (8.39) over the planar transducer surface S. From Eq. (8.19) we would have

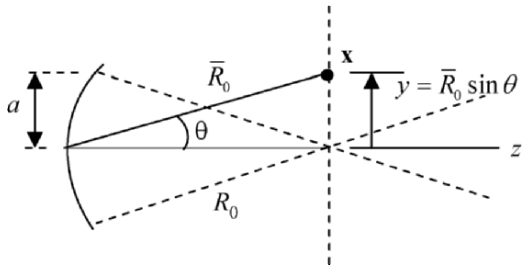

Fig. 8.21. Geometry variables for defining the field behavior at a plane located a distance from the transducer equal to the geometrical focal length.

$$p(\mathbf{x},\omega)=\frac{-i\omega\rho\, v_0(\omega)}{2\pi}\iint_S \exp\left(-ik\rho_0^2/2R_0\right)\frac{\exp(ikr)}{r}dS. \tag{8.40}$$

Consider now the on-axis response. For a circular transducer we can take $dS=2\pi\rho_0 d\rho_0$. But $r=\sqrt{\rho_0^2+z^2}\cong z+\rho_0^2/2z$ in the paraxial approximation so that we obtain an integral that can be done explicitly, giving

$$\begin{aligned} p(z,\omega) &\cong \frac{-i\omega\rho\, v_0(\omega)\exp(ikz)}{z}\int_0^a \exp\left[ik\rho_0^2 q_0/2z\right]\rho_0 d\rho_0 \\ &= \frac{\rho c v_0 \exp(ikz)}{q_0}\left[1-\exp\left(ika^2 q_0/2z\right)\right]. \end{aligned} \tag{8.41}$$

Equation (8.41) is identical to the paraxial result of Eq. (8.38) obtained from the O'Neil model. Thus, in the paraxial approximation, the effect of spherical focusing can be modeled by including a phase term $\exp\left(-ik\rho_0^2/2R_0\right)=\exp\left[-ik\left(x^2+y^2\right)/2R_0\right]$ on the aperture plane $z = 0$ of a planar transducer model. In a similar manner one could introduce bi-cylindrical focusing (different focal lengths R_x and R_y in the x- and y-directions, respectively) by including a phase term of the form $\exp\left[-ik\left(x^2/2R_x+y^2/2R_y\right)\right]$.

8.8 Wave Field in the Plane at the Geometrical Focus

The wave field of a spherically focused piston transducer in a plane located at a distance z = R_0 can also be obtained explicitly from the O'Neil model. One finds (see Fig. 8.21) that [Fundamentals]

$$p(\mathbf{x},\omega)=-i\omega\rho v_0 a^2\frac{\exp\left(ik\bar{R}_0\right)}{\bar{R}_0}\frac{J_1\left(kay/\bar{R}_0\right)}{kay/\bar{R}_0}, \tag{8.42}$$

where $\bar{R}_0$ is the distance from the origin to a point **x** in the wave field. Since for most focused transducers the beam at the geometric focus is confined to a relatively small region near the transducer axis, in most cases

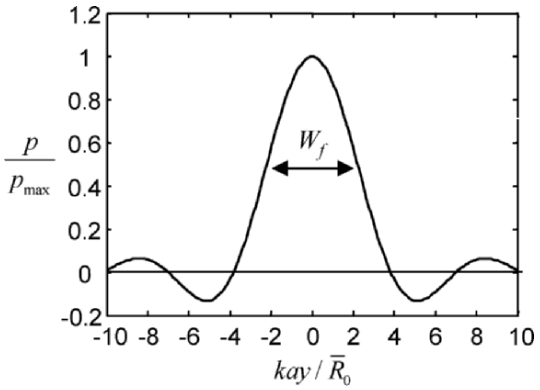

Fig. 8.22. The pressure distribution (due to the $J_1(u)/u$ function) on a plane parallel to the transducer face at a distance from the transducer equal to the geometric focal length.

we can take, approximately, $\overline{R}_0 = R_0$. It is interesting to note that the form of Eq. (8.42) is identical to that of the far field behavior of a circular planar piston transducer (see Eq. (8.31)). In this case, Eq. (8.42) gives us an explicit expression from which we can obtain an estimate of the beam width at the geometric focus. Usually that width is specified as the width of the main lobe when the magnitude of the response has dropped 6 dB from the maximum on-axis response, as shown in Fig. 8.22. Using Eq. (8.42), this beam width is given as [Fundamentals]

$$W_f\Big|_{6\,dB} = 4.43\frac{R_0}{ka} = 1.41\,\lambda\,F \tag{8.43}$$

where $F = R_0/2a$ is called the *transducer F-number*.

8.9 Radiation of a Focused Transducer through an Interface

If one uses a focused transducer in an immersion setup, the transducer beam will be affected by the fluid-solid interface and focus at a shortened distance in the solid, as shown in Fig. 8.23 where a spherically focused piston transducer of radius *a* and focal length R_0 is radiating P-waves at

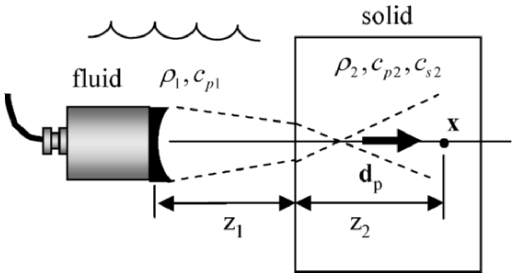

Fig. 8.23. A spherically focused piston transducer radiating a sound beam at normal incidence through a fluid-solid interface.

normal incidence to a planar fluid-solid interface. It can be shown that in the paraxial approximation the on-axis velocity wave field in the solid again can be expressed as a plane wave multiplied by a diffraction coefficient, *C*, i.e.[Fundamentals]

$$\mathbf{v}(\mathbf{x},\omega) = v_0 T_{12}^{P;P} \mathbf{d}_p \exp\left(ik_{p1}z_1 + k_{p2}z_2\right) C\left(z_1, z_2, a, R_0, \omega\right), \tag{8.44}$$

where

$$C\left(z_1, z_2, a, R_0, \omega\right) = \frac{1}{\tilde{q}_0}\left[1 - \exp\left(\frac{ik_{p1}a^2\tilde{q}_0}{2\tilde{z}}\right)\right] \tag{8.45}$$

is of the same form as the diffraction coefficient for the single fluid medium, but with the distance z replaced by $\tilde{z} = z_1 + c_{p2}z_2 / c_{p1}$ as in the planar transducer case and where $\tilde{q}_0 = 1 - \tilde{z}/R_0$.

8.10 Sound Beam in a Solid Generated by a Contact Transducer

All the examples discussed to this point have been for immersion transducers. In contact testing a P-wave transducer, like an immersion transducer, has an element whose motion is primarily normal to the face of the transducer. This transducer is placed in direct contact with the surface of the solid and a small layer of liquid couplant such as water, oil, or glycerin is placed between the transducer and the surface to ensure good coupling of the transducer to the solid. Under these conditions the transducer

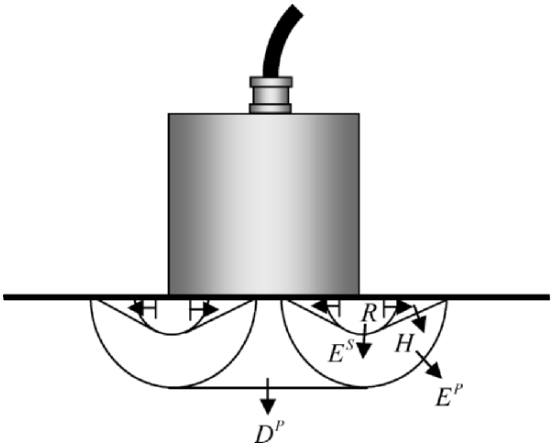

Fig. 8.24. The waves generated by a contact P-wave transducer radiating into a solid.

cannot drive the solid with a piston-like uniform velocity, since the solid is as stiff (or stiffer) than the transducer crystal and its wear plate. Instead, it is more reasonable to assume that the transducer generates a uniform pressure, p_0, over the transducer face. Even though this transducer is called a P-wave transducer, this pressure will actually launch a complicated set of waves of various types, as shown in Fig. 8.24 where a circular P-wave transducer is shown in contact with a stress-free planar surface of a solid. As in the fluid case, there will be a direct P-wave, D^P, that exists in a cylindrical region ahead of the transducer and an edge P-wave, E^P, that radiates from the transducer edge. However, there will also be an edge S-wave, E^S. When the edge P-wave grazes along the stress-free surface, it will generate a "Head" wave, *H*, (also called a von Schmidt wave) that radiates in a conical-like fashion from the interface and links up to the edge S-wave. Finally, the transducer also generates a surface Rayleigh wave, *R*, which moves radially from the transducer along the free surface at a wave speed slightly smaller than the shear wave velocity of the solid and is confined to a region between the free surface and the edge S-wave. Although it appears that the wave field of the contact transducer in Fig. 8.24 is considerably more complicated than the immersion transducer case, not all of the waves in Fig. 8.24 are of equal importance in determining the wave field below the transducer in the solid. The Rayleigh waves, for example, do not affect the wave field except in a region very close to the free surface. The head waves do travel into the solid but they

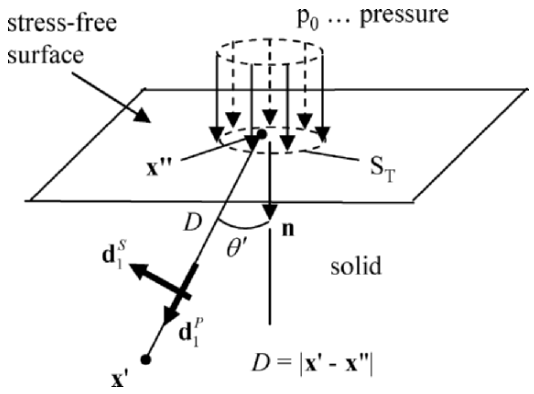

Fig. 8.25. A model of a contact P-wave transducer as a uniform pressure, p_0, acting on the free surface of an elastic solid.

radiate outwards at an angle from the transducer and generally are very weak. Thus, the predominant waves that one needs to consider are the direct P-wave and the edge P-waves and S-waves. A Rayleigh-Sommerfeld integral type of model can also be developed for these direct and edge waves, where the displacement vector, **u**, due to the waves in the solid is given by (see Fig. 8.25) [Fundamentals]

$$\mathbf{u}(\mathbf{x}',\omega)=\frac{p_0}{2\pi\rho_1 c_{s1}^2}\int_{S_T} K_s(\theta')\mathbf{d}_1^s\frac{\exp(ik_{s1}D)}{D}dS(\mathbf{x}'') + \frac{p_0}{2\pi\rho_1 c_{p1}^2}\int_{S_T} K_p(\theta')\,\mathbf{d}_1^p\frac{\exp(ik_{p1}D)}{D}dS(\mathbf{x}''), \tag{8.46}$$

where $D=|\mathbf{x}'-\mathbf{x}''|$, ρ_1 is the density of the solid, the compressional and shear wave speeds are c_{p1}, c_{s1}, respectively, and $\mathbf{d}_1^p, \mathbf{d}_1^s$ are the polarization vectors for the P-waves and S-waves. Unlike the immersion transducer case, the integrals also contain angular dependent directivity functions, $K_p(\theta'), K_s(\theta')$ for the P-waves and S-waves. These functions are given by the expressions [Fundamentals]

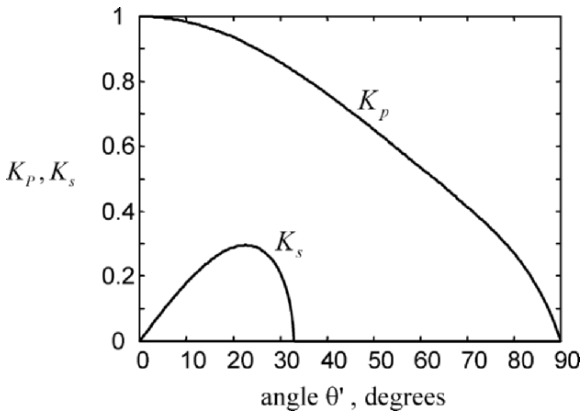

Fig. 8.26. The directivity functions for a contact P-wave transducer.

$$K_p(\theta') = \frac{\cos\theta' \kappa_1^2 \left(\kappa_1^2/2 - \sin^2\theta'\right)}{2G(\sin\theta')}$$
$$K_s(\theta') = \frac{\kappa_1^3 \cos\theta' \sin\theta' \sqrt{1-\kappa_1^2 \sin^2\theta'}}{2G(\kappa_1 \sin\theta')}, \tag{8.47}$$

where $G(x) = \left(x^2 - \kappa_1^2/2\right)^2 + x^2\sqrt{1-x^2}\sqrt{\kappa_1^2 - x^2}$ and $\kappa_1 = c_{p1}/c_{s1}$. The directivities are plotted in Fig. 8.26. Near the central axis of the transducer $K_p \cong 1, K_s \cong 0$ so that Eq. (8.46) reduces to

$$\mathbf{u}(\mathbf{x}', \omega) = \frac{p_0 \mathbf{n}}{2\pi\rho_1 c_{p1}^2} \int_{S_T} \frac{\exp(ik_{p1}D)}{D} dS, \tag{8.48}$$

which now only contains the direct and edge P-waves in a form almost identical to the expression for an immersion transducer. When such a transducer is used to interrogate a material for flaws, it is likely that the response will be "peaked up" by moving the transducer so that the flaw will be on or near the central axis of the transducer. In that case we see from Eq. (8.48) that a Rayleigh-Sommerfeld integral may also be an appropriate model.

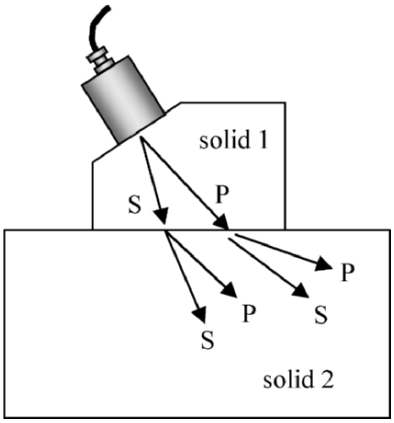

Fig. 8.27. A contact P-wave transducer on a wedge which is contact with another material that is to be inspected.

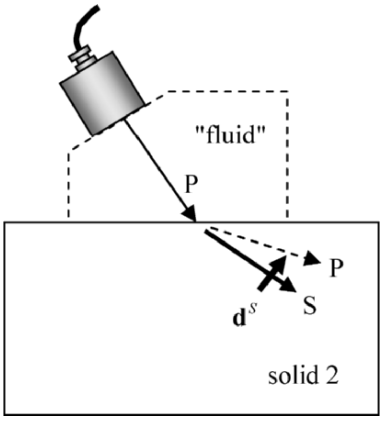

Fig. 8.28. An equivalent "fluid" model of an angle beam shear wave transducer. When the incident P-wave in the wedge is beyond the first critical angle, primarily a refracted S-wave only is generated in the solid with polarization $\mathbf{d}^s$, as shown. Since for the configuration shown $\mathbf{d}^s$ lies in a vertical plane, the S-wave in the solid is called a vertically polarized shear wave (SV-wave). There is a small transmitted P-wave as well in this configuration that can generally be neglected, as indicated by the dashed arrow in the figure.

8.11 Angle Beam Shear Wave Transducer Model

A contact P-wave can also be placed on a solid wedge and used to generate a shear wave in the solid by the process of mode conversion. In general, as shown in Fig. 8.27 the P-wave transducer generates in the wedge primarily the compressional and shear waves we have just discussed. These waves then mode convert to each generate compressional and shear waves in the solid, as shown. However, studies of this configuration have shown that again the only significant wave in the wedge is the compressional wave [Fundamentals]. If the angle of the wedge is chosen so that the compressional wave traveling along the central axis of the transducer is beyond the first critical angle, then primarily a shear wave is generated in the solid, a configuration in which the transducer is called an *angle beam shear wave transducer*. Since the only significant wave in the wedge is the P-wave, an angle beam shear wave transducer can be modeled by replacing the wedge by an equivalent fluid that has the same density and compressional wave speed of the wedge material, as shown in Fig. 8.28 and model the waves transmitted across the interface by using the transmission coefficients for two solids in smooth contact (see Appendix D). Thus, one can use an immersion transducer model as the basis for also modeling an angle beam shear wave transducer.

8.12 Transducer Beam Radiation through Interfaces

In immersion testing, the transducer sound beam inherently must pass through a fluid-solid interface. This causes the beam in the solid to be distorted from its behavior in the fluid. We have seen how at normal incidence to a plane interface we can model the on-axis behavior of these distortions in a simple manner for both planar and spherically focused transducers (see Eqs. (8.25) and (8.44)). For curved interfaces and oblique incidence, the models become much more complex. We can gain some understanding of these cases by using high frequency ray concepts. Consider, for example, a planar piston transducer radiating at oblique incidence to a curved interface, as shown in Fig. 8.29. If we model the wave field in the fluid by a Rayleigh-Sommerfeld integral, then in that model we are radiating a distribution of spherical waves to the interface. From an element of area dS at point $\mathbf{y}$ on the transducer surface a spherical wave generates a pressure at a general point $\mathbf{x}_1$ on the interface given by

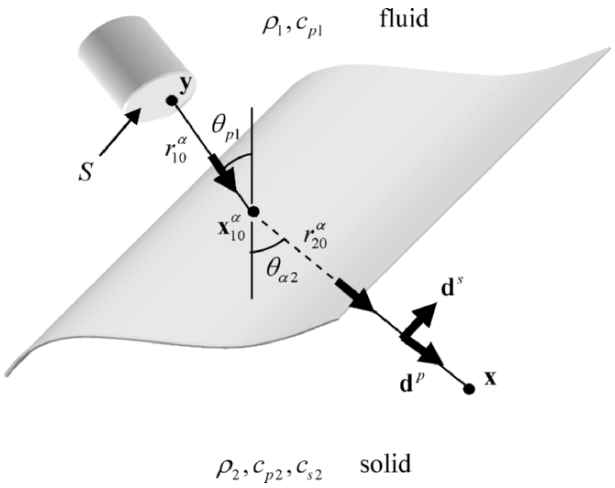

Fig. 8.29. An immersion transducer radiating a sound beam of type α $(\alpha = p, s)$ in a solid through a curved fluid-solid interface, showing a ray path from a point **y** on the transducer surface to a point **x** in the solid through the interface. In the transducer beam model, this ray path must satisfy generalized Snell's law. The polarization of the transmitted waves is defined by the unit vector $\mathbf{d}^{\alpha}$. For a transmitted P-wave, the polarization will be along the direction of propagation while for a transmitted S-wave it will be perpendicular to the direction of propagation. Both polarizations are shown along the refracted ray but for a given wave type only one will be present.

$$dp(\mathbf{x}_1, \omega) = \frac{-i\omega\rho v_0}{2\pi} \frac{\exp(ik_{p1} r_1)}{r_1} dS. \tag{8.49}$$

At high frequencies, the corresponding velocity in this spherical wave is given by

$$d\mathbf{v}(\mathbf{x}_1, \omega) = dv(\mathbf{x}_1, \omega)\mathbf{e}_{p1} = -\mathbf{e}_{p1} \frac{ik_{p1} v_0}{2\pi} \frac{\exp(ik_{p1} r_1)}{r_1} dS, \tag{8.50}$$

where $\mathbf{e}_{p1}$ is a unit vector along a line from point **y** on the transducer face to point $\mathbf{x}_1$ on the interface and $r_1 = |\mathbf{x}_1 - \mathbf{y}|$. By high frequency ray theory, this velocity is propagated into the solid as a bulk wave of type α, where

$\alpha = (p,s)$, to generate a velocity at point **x** in the solid of the form [Fundamentals]

$$d\mathbf{v}^{\alpha}(\mathbf{x},\omega) = \mathbf{d}^{\alpha} dv(\mathbf{x}_{10},\omega) T_{12}^{\alpha;p} \cdot \frac{\sqrt{|\rho_{v1}^{\alpha}|}\sqrt{|\rho_{v2}^{\alpha}|}}{\sqrt{|\rho_{v1}^{\alpha}+r_{20}^{\alpha}|}\sqrt{|\rho_{v2}^{\alpha}+r_{20}^{\alpha}|}} \exp\left(ik_{\alpha 2} r_{20}^{\alpha} + i\phi^{\alpha}\right), \tag{8.51}$$

where $r_{10}^{\alpha} = |\mathbf{x}_{10}^{\alpha} - \mathbf{y}|, r_{20}^{\alpha} = |\mathbf{x} - \mathbf{x}_{10}^{\alpha}|$ are distances from point **y** on the transducer surface to an interface point, $\mathbf{x}_{10}^{\alpha}$ and from that interface point to point **x** in the solid along a ray path that satisfies Snell's law for a wave of type α in the solid (see Fig. 8.29), i.e. we must have

$$\frac{\sin(\theta_{p1})}{c_{p1}} = \frac{\sin(\theta_{\alpha 2})}{c_{\alpha 2}}. \tag{8.52}$$

We will assume that there is only one such path for the present argument, although that may not be true in general for complex curved interfaces. The term $T_{12}^{\alpha;p}$ is just the plane wave transmission coefficient (based on velocity ratios) for a wave of type α in the solid generated by the P-wave in the fluid traveling along this ray path. The factor

$$\frac{\sqrt{|\rho_{v1}^{\alpha}|}\sqrt{|\rho_{v2}^{\alpha}|}}{\sqrt{|\rho_{v1}^{\alpha}+r_{20}^{\alpha}|}\sqrt{|\rho_{v2}^{\alpha}+r_{20}^{\alpha}|}}$$

that appears in Eq. (8.51) involves two "virtual" source distances $\rho_{v1}^{\alpha}, \rho_{v2}^{\alpha}$ and represents the amplitude changes predicted by ray theory. Essentially this factor distorts the incident spherical wave fronts in the fluid to more general curved wave fronts in the solid. Ray theory also predicts that there are additional phase changes, ϕ^{α} in the wave traveling in the solid beyond the term, $k_{\alpha 2} r_{20}^{\alpha}$ due to solely propagation in the solid. The vector $\mathbf{d}^{\alpha}$ in Eq. (8.51) is a unit vector that describes the polarization of the transmitted wave. It is identical to the polarization defined for a transmitted plane wave of type α generated by the interaction of a plane P-wave with a plane interface at point $\mathbf{x}_{10}^{\alpha}$ where the normal to the plane interface coincides with the actual interface normal of the curved interface at that point.

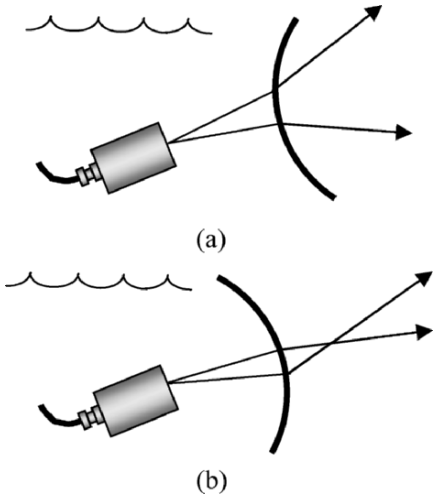

Fig. 8.30. (a) A planar transducer radiating through a curved fluid-solid interface that spreads (defocuses) the waves in the solid, and **(b)** a curved interface that focuses the waves in the solid.

By integrating the expression in Eq. (8.51) over the face of the transducer one then obtains a beam model for the total velocity in the transmitted waves:

$$\mathbf{v}^{\alpha}\left(\mathbf{x},\omega\right)=\int_{S}\Big[\ \mathbf{d}^{\alpha}T_{12}^{\alpha;p}\frac{\sqrt{\left|\rho_{v1}^{\alpha}\right|}\sqrt{\left|\rho_{v2}^{\alpha}\right|}}{\sqrt{\left|\rho_{v1}^{\alpha}+r_{20}^{\alpha}\right|}\sqrt{\left|\rho_{v2}^{\alpha}+r_{20}^{\alpha}\right|}}\exp\left(ik_{\alpha 2}r_{20}^{\alpha}+i\phi^{\alpha}\right)dv\left(\mathbf{x}_{10},\omega\right)\Big]. \tag{8.53}$$

There are, however, some difficulties with this model [Fundamentals]. As long as the curved interface is of a defocusing type, as shown in Fig. 8.30 (a), where the rays from a point on the transducer surface traveling into the solid do not touch or cross, Eq. (8.53) is well-behaved and can be used, like the Rayleigh-Sommerfeld equation, to calculate the sound beam in the solid. However, if the curved interface is of a focusing type, as shown in Fig. 8.30 (b), the rays can touch or cross and the ray theory amplitude term becomes infinite. There are uniform ray theory approximations that can remove those singularities but the analysis and resulting expressions become much more complex. This difficulty arises mathematically because we have modeled the transducer beam as a

superposition of spherical waves arising from point sources, and spherical waves can become singular, for example, when focused at a point by a curved interface. Similar focusing singularities can occur for plane waves incident on a curved interface so that an angular plane wave spectrum model will also have these same difficulties when focusing curved interfaces are present. In the next Chapter, we will show that these problems can be eliminated by expanding the transducer wave field in terms of Gaussian beams which always remain non-singular.

There is an important special case when Eq. (8.53) is always well-behaved [Fundamentals]. That case is when the planar piston transducer is incident at oblique incidence on a planar interface. In that case we have $\phi^{\alpha} = 0$ and

$$\begin{aligned} \rho_{v1}^{\alpha} &= \frac{c_{p1}\cos^2\left(\theta_{\alpha 2}\right)}{c_{\alpha 2}\cos^2\left(\theta_{p1}\right)} r_{10}^{\alpha} \\ \rho_{v2}^{\alpha} &= \frac{c_{p1}}{c_{\alpha 2}} r_{10}^{\alpha} \end{aligned} \tag{8.54}$$

so Eq. (8.53) becomes, explicitly,

$$\begin{aligned} \mathbf{v}^{\alpha}\left(\mathbf{x},\omega\right) = \frac{-ik_{p1}v_0}{2\pi}\int_S \Big[T_{12}^{\alpha;p}\mathbf{d}^{\alpha} \\ \cdot \frac{\exp\left(ik_{p1}r_{10}^{\alpha} + ik_{\alpha 2}r_{20}^{\alpha}\right)}{\sqrt{r_{10}^{\alpha} + \left(c_{\alpha 2}^2/c_{p1}^2\right)r_{20}^{\alpha}}\sqrt{r_{10}^{\alpha} + \left(c_{\alpha 2}^2\cos^2\theta_{p1}/c_{p1}^2\cos^2\theta_{\alpha 2}\right)r_{20}^{\alpha}}} \Big] dS. \end{aligned} \tag{8.55}$$

Equation (8.55) is in a form very similar to the Rayleigh-Sommerfeld equation. Instead of superimposing spherical waves traveling directly from the transducer to the point in the fluid, we now need to superimpose a more general set of waves with elliptical wave fronts in the solid that travel along rays satisfying Snell's law and are modified by the plane wave transmission coefficient of the interface. Since both that transmission coefficient and the polarization vector depend on that ray path, they are both implicit functions of point **y** on the transducer surface and so must remain inside the integral. In general the integral in Eq. (8.55) must be performed numerically, so that like the Rayleigh-Sommerfeld integral the highly oscillatory complex exponentials in Eq. (8.55) make this evaluation a rather intensive computation. Fortunately, the Gaussian beam models discussed in the next Chapter will also be much more numerically efficient than these types of Rayleigh-Sommerfeld integral models.

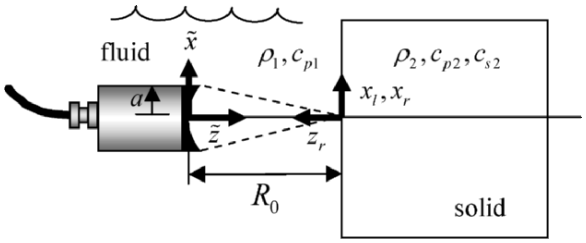

Fig. 8.31. An experimental setup for a spherically focused transducer of radius a and focal length R_0 where one can obtain the acoustic/elastic transfer function explicitly.

8.13 Acoustic/Elastic Transfer Function – Focused Transducer

In Chapter 7 it was shown that the acoustic/elastic transfer function is needed in order to determine experimentally the system function. In Chapter 6 the acoustic/elastic transfer function also played a key role in determining the transducer sensitivity. In Chapter 5 we obtained an acoustic/elastic transfer function for both a pitch-catch and a pulse-echo immersion setup. In Chapter 13 a general procedure is given for using a multi-Gaussian beam model to determine the acoustic/elastic transfer function in cases where the transfer function cannot be obtained analytically (angle beam testing and contact testing setups with curved surfaces, etc.). A number of other acoustic/elastic transfer functions can be derived from results given in [Fundamentals]. All of those cases, however, are for planar piston transducers. The acoustic/elastic transfer function for a spherically focused piston transducer in a pulse-echo immersion configuration is also available [8.4], [8.5], a case we will develop here as a simple application of the paraxial approximation and the use of the phase term discussed in Eq. (8.39). This approach will also lead to the transfer function for planar and cylindrically focused rectangular piston transducers in the following section.

The configuration we will consider is the pulse-echo setup shown in Fig. 8.31 where a spherically focused piston transducer of radius a and focal length, R_0, radiates waves into a fluid and receives the waves reflected from a plane fluid-solid interface. The distance from the transducer to interface is made equal to the geometrical focal length in this configuration.

As discussed in section 8.7, in the paraxial approximation we can use the Rayleigh-Sommerfeld equation to represent the wave field of a spherically focused transducer in the form (see Eq. (8.40))

$$p(\mathbf{x},\omega)=\frac{-i\omega\rho_1\, v_0(\omega)}{2\pi}\iint_S \exp\left[-ik_{p1}\left(\tilde{x}^2+\tilde{y}^2\right)/2R_0\right] \cdot\frac{\exp\left(ik_{p1}r\right)}{r}dS, \tag{8.56}$$

where $(\tilde{x},\tilde{y},\tilde{z}=0)$ are coordinates of a point on a plane at the transmitting transducer and $r=\sqrt{(\tilde{x}-x_l)^2+(\tilde{y}-y_l)^2+z_l^2}$ is the distance from that point to a point (x_l,y_l,z_l) in the fluid. Let the point in the fluid lie on the interface as shown in Fig. 8.31. Then $r=\sqrt{(\tilde{x}-x_l)^2+(\tilde{y}-y_l)^2+R_0^2}$ .We also apply the paraxial approximation to this distance function to obtain $r\cong R_0+\left[(\tilde{x}-x_l)^2+(\tilde{y}-y_l)^2\right]/2R_0$ and Eq. (8.56) becomes

$$p(x_l,y_l,R_0,\omega)=\frac{-i\omega\rho_1\, v_0(\omega)\exp\left(ik_{p1}R_0\right)}{2\pi R_0} \cdot\iint_S \exp\left[-ik_{p1}\frac{\left(\tilde{x}^2+\tilde{y}^2\right)}{2R_0}\right]\exp\left[ik_{p1}\frac{(\tilde{x}-x_l)^2+(\tilde{y}-y_l)^2}{2R_0}\right]d\tilde{x}d\tilde{y}. \tag{8.57}$$

Equation (8.57) is in the form of a quasi-plane wave so at high frequencies the pressure in the reflected wave at the interface, $p_R(x_l,y_l,R_0,\omega)$, can be obtained by the plane wave relationship

$$\begin{aligned} p_R(x_l,y_l,R_0,\omega)&=R_{12}p(x_l,y_l,R_0,\omega)\\ &=\frac{\rho_2c_{p2}-\rho_1c_{p1}}{\rho_2c_{p2}+\rho_1c_{p1}}p(x_l,y_l,R_0,\omega), \end{aligned} \tag{8.58}$$

where R_{12} is the reflection coefficient (based on a pressure ratio). The normal velocity at the interface in the z_r direction, v_r, (see Fig. 8.31) is also given by the plane wave relationship

$$v_r(x_l,y_l,R_0,\omega)=R_{12}p(x_l,y_l,R_0,\omega)/\rho_1c_{p1}. \tag{8.59}$$

Using this velocity field as specified on the entire interface, we can again use the Rayleigh-Sommerfeld integral (with the paraxial approximation applied again to the radius, *r*, in that integral) to obtain the reflected waves that are incident on the transducer from the interface. We find

$$p(x_r, y_r, z_r, \omega) = \frac{-ik_{p1}R_{12}\exp(ikz_r)}{2\pi z_r}\int_{-\infty}^{+\infty}\int_{-\infty}^{+\infty} p(x_l, y_l, R_0, \omega) \cdot \exp\left[ik_{p1}\frac{(x_r - x_l)^2 + (y_r - y_l)^2}{2z_r}\right] dx_l dy_l. \tag{8.60}$$

For a spherically focused transducer, this pressure is received not at the plane $z_r = R_0$ but instead over the curved spherical surface given by $z_r = R_0 - \left(x_r^2 + y_r^2\right)/2R_0$. Placing this distance into the plane wave phase term in Eq. (8.60) (and using $z_r = R_0$ elsewhere in Eq. (8.60)), the average pressure, p_{ave}, over the area, *S*, of the transducer is given by

$$p_{ave} = \frac{-ik_{p1}R_{12}\exp(ikR_0)}{2\pi R_0 S}\iint_S \exp\left[-ik_{p1}\frac{\left(x_r^2 + y_r^2\right)}{2R_0}\right] \left\{\int_{-\infty}^{+\infty}\int_{-\infty}^{+\infty} p(x_l, y_l, R_0, \omega)\exp\left[ik_{p1}\frac{(x_r - x_l)^2 + (y_r - y_l)^2}{2R_0}\right] \cdot dx_l dy_l \right\} dx_r dy_r. \tag{8.61}$$

Substituting the expression for the pressure at the interface (Eq. (8.57)) into Eq. (8.61), we obtain an explicit expression for the average pressure acting on the transducer. Then from this average pressure we can find the blocked force, $F_B = 2p_{ave}S$, received by the transducer as

$$
\begin{aligned}
F_B &= 2R_{12}\exp\left(2ik_{p1}R_0\right)\frac{-ik_{p1}}{2\pi R_0}\frac{-ik_{p1}\rho_1 c_{p1}v_0}{2\pi R_0} \\
&\cdot\iint_S\left(\iint_S \exp\left[-ik_{p1}\frac{\left(x_r^2+y_r^2\right)}{2R_0}\right]\exp\left[-ik_{p1}\frac{\left(\tilde{x}^2+\tilde{y}^2\right)}{2R_0}\right]\right. \\
&\cdot\left[\int_{-\infty}^{+\infty}\int_{-\infty}^{+\infty}\exp\left[ik_{p1}\frac{\left(x_r-x_l\right)^2+\left(y_r-y_l\right)^2}{2R_0}\right]\right. \\
&\left.\left.\exp\left[ik_{p1}\frac{\left(\tilde{x}-x_l\right)^2+\left(\tilde{y}-y_l\right)^2}{2R_0}\right]dx_l dy_l\right]dx_r dy_r\right)d\tilde{x}d\tilde{y}.
\end{aligned}
\tag{8.62}
$$

Since $F_t = \rho_1 c_{p1} S v_0$ is the force transmitted by the transducer acting as a transmitter, the acoustic/elastic transfer function for our focused transducer, $t_A^{foc} = F_B / F_t$ is given by

$$
\begin{aligned}
t_A^{foc} &= 2R_{12}\exp\left(2ik_{p1}R_0\right)\frac{-ik_{p1}}{2\pi R_0 S}\frac{-ik_{p1}}{2\pi R_0} \\
&\cdot\iint_S\left(\iint_S \exp\left[-ik_{p1}\frac{\left(x_r^2+y_r^2\right)}{2R_0}\right]\exp\left[-ik_{p1}\frac{\left(\tilde{x}^2+\tilde{y}^2\right)}{2R_0}\right]\right. \\
&\cdot\left[\int_{-\infty}^{+\infty}\int_{-\infty}^{+\infty}\exp\left[ik_{p1}\frac{\left(x_r-x_l\right)^2+\left(y_r-y_l\right)^2}{2R_0}\right]\right. \\
&\left.\left.\exp\left[ik_{p1}\frac{\left(\tilde{x}-x_l\right)^2+\left(\tilde{y}-y_l\right)^2}{2R_0}\right]dx_l dy_l\right]dx_r dy_r\right)d\tilde{x}d\tilde{y}.
\end{aligned}
\tag{8.63}
$$

Equation (8.63) is a rather formidable looking expression, but we can proceed as follows. First, we note that the acoustic/elastic transfer function for a planar transducer of the same size as our spherically focused transducer, t_A^{planar} is given by exactly the same expression as Eq. (8.63) without the first two phase terms:

$$t_A^{planar} = 2R_{12}\exp\left(2ik_{p1}R_0\right)\frac{-ik_{p1}}{2\pi R_0 S}\frac{-ik_{p1}}{2\pi R_0}$$
$$\cdot\iint_S\left(\iint_S\left[\int_{-\infty}^{+\infty}\int_{-\infty}^{+\infty}\exp\left[ik_{p1}\frac{\left(x_r-x_l\right)^2+\left(y_r-y_l\right)^2}{2R_0}\right]\right.\right. \tag{8.64}$$
$$\left.\left.\cdot\exp\left[ik_{p1}\frac{\left(\tilde{x}-x_l\right)^2+\left(\tilde{y}-y_l\right)^2}{2R_0}\right]dx_l dy_l\right]dx_r dy_r\right)d\tilde{x}d\tilde{y}.$$

In Eqs. (8.63) and (8.64) the integrals over the interface are identical for the focused and planar cases. These integrals can be rewritten as

$$I = \int_{-\infty}^{+\infty}\int_{-\infty}^{+\infty}\exp\left[ik_{p1}\frac{\left(x_r-x_l\right)^2+\left(y_r-y_l\right)^2}{2R_0}\right]$$
$$\cdot\exp\left[ik_{p1}\frac{\left(\tilde{x}-x_l\right)^2+\left(\tilde{y}-y_l\right)^2}{2R_0}\right]dx_l dy_l$$
$$= \exp\left(ik_{p1}\frac{\left(x_r^2+y_r^2\right)}{2R_0}\right)\exp\left(ik_{p1}\frac{\left(\tilde{x}^2+\tilde{y}^2\right)}{2R_0}\right) \tag{8.65}$$
$$\cdot\int_{-\infty}^{+\infty}\exp\left(ik_{p1}\frac{x_l^2}{R_0}\right)\exp\left(-ik_{p1}\frac{\left(\tilde{x}+x_r\right)x_l}{R_0}\right)dx_l$$
$$\cdot\int_{-\infty}^{+\infty}\exp\left(ik_{p1}\frac{y_l^2}{R_0}\right)\exp\left(-ik_{p1}\frac{\left(\tilde{y}+y_r\right)y_l}{R_0}\right)dy_l$$

The remaining integrals can be performed exactly because we have [8.2]

$$\int_{-\infty}^{+\infty}\exp\left(iAx^2\right)\exp\left(-iBx\right)dx = \sqrt{\frac{i\pi}{A}}\exp\left(\frac{-iB^2}{4A}\right), \tag{8.66}$$
$$\mathrm{Im}\left[A\right] > 0$$

where Im[ ] indicates "imaginary part of ". In Eq. (8.65) the corresponding A terms are purely real but if we add a small amount of "damping" by letting $A = A + i\varepsilon$ and then take the limit as $\varepsilon \to 0$, the result is the same as using Eq. (8.66) directly on the forms given in Eq. (8.65) and we find

$$I = \frac{i\pi R_0}{k_{p1}} \exp\left(ik_{p1} \frac{\left(x_r^2 + y_r^2\right)}{2R_0} \right) \exp\left(ik_{p1} \frac{\left(\tilde{x}^2 + \tilde{y}^2\right)}{2R_0} \right) \cdot \exp\left(-ik_{p1} \frac{\left(\tilde{x} + x_r\right)^2}{4R_0} \right) \exp\left(-ik_{p1} \frac{\left(\tilde{y} + y_r\right)^2}{4R_0} \right). \tag{8.67}$$

In the focused case, we see that the first two phase terms in Eq. (8.67) simply cancel the first two phase terms in Eq. (8.63) and we obtain

$$t_A^{foc} = 2R_{12} \exp\left(2ik_{p1}R_0\right) \frac{-ik_{p1}}{4\pi R_0 S} \iint_S \left(\iint_S \exp\left[-ik_{p1} \frac{\left(\tilde{x} + x_r\right)^2}{4R_0} \right] \cdot \exp\left[-ik_{p1} \frac{\left(\tilde{y} + y_r\right)^2}{4R_0} \right] dx_r dy_r \right) d\tilde{x} d\tilde{y}. \tag{8.68}$$

However, we note that for a circular, spherically focused transducer the integrations in Eq. (8.68) are over symmetrical intervals in both x_r and y_r so that we can make the replacements $x_r \to -x_r$ and $y_r \to -y_r$ in Eq. (8.68) without affecting the end result. With those, replacements, we have, finally,

$$t_A^{foc} = 2R_{12} \exp\left(2ik_{p1}R_0\right) \frac{-ik_{p1}}{4\pi R_0 S} \iint_S \left(\iint_S \exp\left[-ik_{p1} \frac{\left(\tilde{x} - x_r\right)^2}{4R_0} \right] \exp\left[-ik_{p1} \frac{\left(\tilde{y} - y_r\right)^2}{4R_0} \right] dx_r dy_r \right) d\tilde{x} d\tilde{y} \tag{8.69}$$

In the planar transducer case, we can place Eq. (8.67) into Eq. (8.64) to find

$$t_A^{planar} = 2R_{12}\exp\left(2ik_{p1}R_0\right)\frac{-ik_{p1}}{4\pi R_0 S}\iint_S\left(\iint_S \exp\left(ik_{p1}\frac{\left(x_r^2+y_r^2\right)}{2R_0}\right)\right.$$
$$\cdot\exp\left(ik_{p1}\frac{\left(\tilde{x}^2+\tilde{y}^2\right)}{2R_0}\right)\exp\left(-ik_{p1}\frac{\left(\tilde{x}+x_r\right)^2}{4R_0}\right) \tag{8.70}$$
$$\left.\cdot\exp\left(-ik_{p1}\frac{\left(\tilde{y}+y_r\right)^2}{4R_0}\right)dx_r dy_r\right)d\tilde{x}d\tilde{y},$$

which, when the exponential terms are combined, gives

$$t_A^{planar} = 2R_{12}\exp\left(2ik_{p1}R_0\right)\frac{-ik_{p1}}{4\pi R_0 S}$$
$$\cdot\iint_S\left(\iint_S \exp\left(ik_{p1}\frac{\left(\tilde{x}-x_r\right)^2}{4R_0}\right)\right. \tag{8.71}$$
$$\left.\cdot\exp\left(ik_{p1}\frac{\left(\tilde{y}-y_r\right)^2}{4R_0}\right)dx_r dy_r\right)d\tilde{x}d\tilde{y}.$$

In Chapter 5, we obtained an explicit expression for acoustic/elastic transfer function for the planar transducer case. For the geometry of Fig. 8.31 we can write the transfer function for a planar transducer in terms of the diffraction correction, $\tilde{D}_p$, used in Chapter 5 (see Eq. (5.20)) as

$$t_A^{planar}(\omega) = \tilde{D}_p\left(k_{p1}a^2/2R_0\right)R_{12}\exp\left(2ik_{p1}R_0\right), \tag{8.72}$$

where

$$\tilde{D}_p(u) = 2\left[1-\exp(iu)\left\{J_0(u)-iJ_1(u)\right\}\right]. \tag{8.73}$$

Comparing Eqs. (8.69) and (8.71) and using Eq. (8.72) for the planar case, we see that for the focused case we have

$$t_A^{foc}(\omega) = -\left[\tilde{D}_p\left(k_{p1}a^2/2R_0\right)\right]^* R_{12}\exp\left(2ik_{p1}R_0\right) \tag{8.74}$$

where $[\ ]^*$ denotes the "complex conjugate". Thus, by making the changes indicated by Eq. (8.74) one can simply use the same diffraction correction obtained for the planar case for this focused case as well. Note, however, that while in the planar transducer case the interface is not restricted to

being at a particular distance from the transducer the interface *must* be placed at the geometrical focal length of the focused transducer in order to use Eq. (8.74).

8.14 Acoustic/Elastic Transfer Function – Rectangular Transducer

The results of the previous section can also be used to obtain the acoustic/elastic transfer function for a rectangular piston transducer that is either planar or cylindrically focused and receiving the waves reflected from the front surface of a block (same setup as shown in Fig. 8.31). First, consider a planar rectangular transducer of length $2a$ in the $\tilde{x}$-direction and $2b$ in the $\tilde{y}$-direction and let the distance $R_0 = D$ (see Fig. 8.31). Then from Eq. (8.71) the acoustic/elastic transfer function, t_A^{rect}, is

$$\begin{aligned} t_A^{rect} &= 2R_{12}\exp\left(2ik_{p1}D\right)\frac{-ik_{p1}}{16\pi Dab} \\ &\cdot\int_{-b}^{+b}\int_{-a}^{+a}\left(\int_{-b}^{+b}\int_{-a}^{+a}\exp\left(ik_{p1}\frac{\left(\tilde{x}-x_r\right)^2}{4D}\right)\right. \\ &\left.\cdot\exp\left(ik_{p1}\frac{\left(\tilde{y}-y_r\right)^2}{4D}\right)dx_r dy_r\right)d\tilde{x}d\tilde{y}. \end{aligned} \tag{8.75}$$

But in this case we have

$$\int_{-a}^{+a}\int_{-a}^{+a}\exp\left(ik_{p1}\frac{\left(\tilde{x}-x_r\right)^2}{4D}\right)dx_r d\tilde{x} = \frac{4\pi D}{k_{p1}}\int_0^{\sqrt{2ka^2/\pi D}}F\left(x\right)dx, \tag{8.76}$$

where $F\left(x\right)$ is the Fresnel integral

$$F\left(x\right) = \int_0^x \exp\left(i\pi t^2/2\right)dt. \tag{8.77}$$

and similarly

$$\int_{-b}^{+b}\int_{-b}^{+b}\exp\left(ik_{p1}\frac{\left(\tilde{y}-y_r\right)^2}{4D}\right)dy_r d\tilde{y} = \frac{4\pi D}{k_{p1}}\int_0^{\sqrt{2kb^2/\pi D}}F\left(x\right)dx. \tag{8.78}$$

For the integral of the Fresnel function we can use the relationship [8.6] (which comes directly from integration by parts)

$$\int_{x_1}^{x_2} F(x)\,dx = \left[x\,F(x) + \frac{i}{\pi}\exp\left(i\pi x^2/2\right) \right]_{x_1}^{x_2} \tag{8.79}$$

to obtain

$$\begin{aligned} t_A^{rect} = R_{12}\exp\left(2ik_{p1}D\right)\frac{4}{i}\Bigg\{ & F\left(\sqrt{2k_{p1}a^2/\pi D}\right) + \\ & \frac{i}{\pi\sqrt{2k_{p1}a^2/\pi D}}\left[\exp\left(ik_{p1}a^2/D\right)-1\right]\Bigg\} \\ \cdot\Bigg\{ & F\left(\sqrt{2k_{p1}b^2/\pi D}\right) + \frac{i}{\pi\sqrt{2k_{p1}b^2/\pi D}}\left[\exp\left(ik_{p1}b^2/D\right)-1\right]\Bigg\}. \end{aligned} \tag{8.80}$$

We can express Eq. (8.80) in terms of a diffraction correction term, $\tilde{D}_p^{rect}$, where

$$\begin{aligned} \tilde{D}_p^{rect} = \frac{4}{i}\Bigg\{ & F\left(\sqrt{2k_{p1}a^2/\pi D}\right) + \\ & \frac{i}{\pi\sqrt{2k_{p1}a^2/\pi D}}\left[\exp\left(ik_{p1}a^2/D\right)-1\right]\Bigg\} \\ \cdot\Bigg\{ & F\left(\sqrt{2k_{p1}b^2/\pi D}\right) + \frac{i}{\pi\sqrt{2k_{p1}b^2/\pi D}}\left[\exp\left(ik_{p1}b^2/D\right)-1\right]\Bigg\} \end{aligned} \tag{8.81}$$

so that

$$t_A^{rect}(\omega) = \tilde{D}_p^{rect}\left(k_{p1}a^2/2D\right)R_{12}\exp\left(2ik_{p1}D\right). \tag{8.82}$$

Figure 8.32 shows a plot of $\tilde{D}_p^{rect}$ versus frequency for a rectangular transducer where $D = 50.8$ mm and $a = 12.7$ mm, $b = 6.35$ mm. For comparison the corresponding diffraction correction for a 12.7 mm radius circular transducer (Eq. 8.73) is also plotted in Fig. 8.32. It can be see that the rectangular transducer has a very similar behavior to the circular probe and that both diffraction corrections asymptotically approach a value of two for high frequencies.

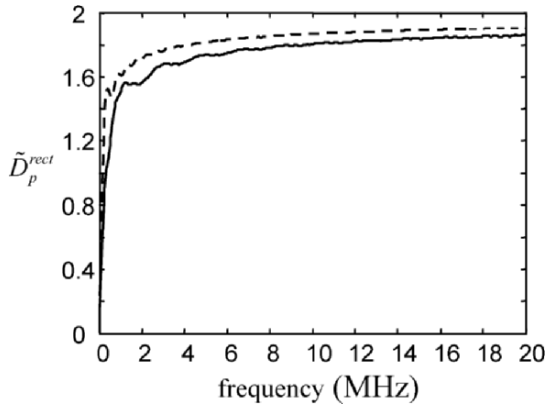

Fig. 8.32. The diffraction correction, $\tilde{D}_p^{rect}$, for a rectangular 25.4 x 12.7 mm rectangular transducer (solid line) and the corresponding diffraction correction, $\tilde{D}_p$, for a 12.7 mm radius circular transducer (dashed line). In both cases the distance D = 50.8 mm.

We can also consider a rectangular cylindrically focused transducer in the same fashion as done for the spherically focused transducer. For a transducer with cylindrical focusing of radius R in the $\tilde{y}$-direction, we can introduce the phase term $\exp\left(-ik_{p1}\tilde{y}^2/2R\right)$ into the Rayleigh-Sommerfeld equation and follow the same steps as in the spherically focused transducer case to obtain the acoustic/elastic transfer function, t_A^{cyl}, in the form

$$t_A^{cyl} = 2R_{12}\exp\left(2ik_{p1}R\right)\frac{-ik_{p1}}{16\pi Rab}\int_{-b}^{+b}\int_{-a}^{+a}\left(\int_{-b}^{+b}\int_{-a}^{+a}\exp\left(ik_{p1}\frac{\left(\tilde{x}-x_r\right)^2}{4R}\right)\right.$$
$$\left.\cdot\exp\left(ik_{p1}\frac{\left(\tilde{y}+y_r\right)^2}{4R}\right)dx_r dy_r\right)d\tilde{x}d\tilde{y}, \tag{8.83}$$

where we must set the distance, $D = R$, as in the spherically focused case. Again, we can express these integrations in terms of Fresnel integrals. Since the details are the same as for the planar case, we just give the end result, namely

$$t_A^{cyl} = R_{12}\exp\left(2ik_{p1}R\right)\frac{4}{i}\left\{F\left(\sqrt{2k_{p1}a^2/\pi R}\right)+\right.$$
$$\left.\frac{i}{\pi\sqrt{2k_{p1}a^2/\pi R}}\left[\exp\left(ik_{p1}a^2/R\right)-1\right]\right\} \tag{8.84}$$
$$\cdot\left\{F\left(\sqrt{2k_{p1}b^2/\pi R}\right)+\frac{i}{\pi\sqrt{2k_{p1}b^2/\pi R}}\left[\exp\left(ik_{p1}b^2/R\right)-1\right]\right\}^*,$$

where again $\{\ \}^*$ indicates the complex conjugate.

8.15 References

8.1 Stamnes JJ (1986) Waves in focal regions. Institute of Physics Publishing, Bristol, England
8.2 Gaskill JD (1978) Linear systems, Fourier transforms and optics. John Wiley and Sons, New York, NY
8.3 O'Neil HT (1949) Theory of focusing radiators. J. Acoust. Soc. Am. 21: 516-526
8.4 Thompson RB, Gray TA (1982) Range of applicability of inversion algorithms. In: Thompson DO, Chimenti DE (eds) Review of progress in quantitative nondestructive evaluation 1, Plenum Press, New York, NY, pp 233-248
8.5 Chen X, Schwartz KQ (1994) Acoustic coupling from a focused transducer to a flat plate and back to the transducer. J. Acoust. Soc. Am. 95: 3049-3054
8.6 Abramowitz M, Stegun IA (1965) Handbook of mathematical functions. Dover Publications, New York, NY

8.16 Exercises

1. The exact on-axis pressure for a circular piston transducer was given by Eq. (8.20) and the far field approximation for this same pressure was given by Eq. (8.21). Using MATLAB, write a script that computes these two pressure expressions and plots the magnitude of the normalized pressure, $p/\rho c v_0$, versus the normalized distance, z/N, for both of these expressions on the same plot, where N is the near field distance. Let the transducer radius a = 6.35 mm, the frequency f = 5 MHz, and the wave speed of the fluid c = 1480 m/sec. Show both pressure plots over the range z/N = 0.2 to

$z/N = 4.0$. What can you conclude about when Eq. (8.21) is valid?

2. Equation (8.31) shows that the angular distribution of the far field radiation field of a circular planar piston transducer is controlled by the directivity function $J_1(ka\sin\theta)/(ka\sin\theta)$. Using MATLAB, write a function that calculates the angle where the amplitude of this directivity function drops by 6 dB from its maximum on-axis value. Use this function to determine the 6 dB angular spread of a 0.5 inch diameter piston transducer radiating into water at frequencies of 2.25, 5, and 10 MHz.

3. Equation (8.19) is the Rayleigh-Sommerfeld integral for a planar piston transducer radiating into a fluid. Consider this equation for a rectangular transducer with width $2a$ in the x-direction and width $2b$ in the y-direction. In the paraxial (Fresnel) approximation we can approximate the radius $r = \sqrt{z^2 + (x-x')^2 + (y-y')^2}$ appearing in the denominator of that equation as $r \cong R = \sqrt{x^2 + y^2 + z^2}$, where (x, y, z) is a point in the fluid and $(x', y', 0)$ is a point on the transducer face. In the phase term of Eq. (8.19), however, we approximate the radius r instead as

$$r = z\sqrt{1 + \frac{(x-x')^2}{z^2} + \frac{(y-y')^2}{z^2}}$$
$$\cong z + \frac{(x-x')^2}{2z} + \frac{(y-y')^2}{2z}$$

Thus, with these approximations Eq. (8.19) for a rectangular transducer is:

$$p = \frac{-i\omega\rho v_0}{2\pi R}\exp(ikz)\int_{-a}^{+a}\exp\left[\frac{ik(x-x')^2}{2z}\right]dx'\int_{-b}^{+b}\exp\left[\frac{ik(y-y')^2}{2z}\right]dy'$$

Show that this expression can be written as the product of the difference of two Fresnel integrals in the form

$$\frac{p}{\rho c v_0} = \frac{-iz}{2R}\exp(ikz)\left[F\left(\sqrt{\frac{k}{\pi z}}(x+a)\right) - F\left(\sqrt{\frac{k}{\pi z}}(x-a)\right)\right]$$
$$\cdot\left[F\left(\sqrt{\frac{k}{\pi z}}(y+b)\right) - F\left(\sqrt{\frac{k}{\pi z}}(y-b)\right)\right]$$

where $F(x)$ is the Fresnel integral as defined in Eq. (8.77). Using the MATLAB function fresnel_int and the above expression, write a MATLAB function that computes this pressure wave field at any point (x, y, z) in the fluid. For a 6mm by 12mm rectangular transducer radiating into water (c = 1480 m/sec) at 5 MHz, plot the magnitude of the normalized on-axis pressure for distances z = 6 mm to z = 100 mm. For the same transducer plot cross-axis pressure profiles in the x- and y-directions at z = 45, 70 mm.

4. Write a MATLAB function that returns the normalized on-axis pressure, $p/\rho c v_0$, versus distance for a spherically focused piston transducer (see Eq. (8.37)). The input arguments of the function should be the distance values (in mm), the frequency (in MHz), the radius (in mm), the geometrical focal length (in mm), and the wave speed (in m/sec). Use this function to find the location of the true focus (i.e. the distance to the maximum pressure) for a 12.7 mm (0.5 inch) diameter, 101.6 mm (4 in.) focal length transducer radiating into water at 5, 10, and 20 MHz. What can you conclude about the relationship between the location of the true focus versus the geometrical focal length?

5. Equation (8.20) gives the exact on-axis pressure for a planar immersion transducer at a single frequency. Ultrasonic NDE transducers, however, do not normally operate at a single frequency but are driven by a voltage pulse and hence contain a spectrum of frequencies that generate a time domain pulse. The near field behavior of such a pulsed transducer does not show nearly the same strong near field structure as a single frequency model suggests.

Write a MATLAB function that computes the normalized pressure, $p/\rho c v_0$, at a given on-axis distance at many frequencies and multiplies this pressure at each frequency by the MATLAB function spectrum1 written for exercise 1 in Appendix A. The function should evaluate this product at 1024 positive frequencies ranging from 0 to 100 MHz and then use the Fourier transform IFourierT defined in Appendix A to obtain the time-domain pulse generated by the transducer at the given location. Finally, the function should compute the peak-to-peak magnitude of this pulse and return that value. The inputs to the MATLAB function should be the distance (in mm), the transducer radius (in mm), the wave speed of the fluid (in m/sec), the center frequency, fc (in MHz), and the bandwidth, bw (in MHz).

Use this function to evaluate the peak-to peak response of a transducer radiating into water for 200 points ranging from 10 to 400 mm and plot this peak-to-peak response versus distance. Take the radius of the transducer to be 6.35 mm (0.25 in.), the center frequency fc = 5 MHz and the bandwidth bw = 2 MHz.